iScience

CellPress
OPEN ACCESS

Article

AUTS2 Governs Cerebellar Development, Purkinje Cell Maturation, Motor Function and Social Communication

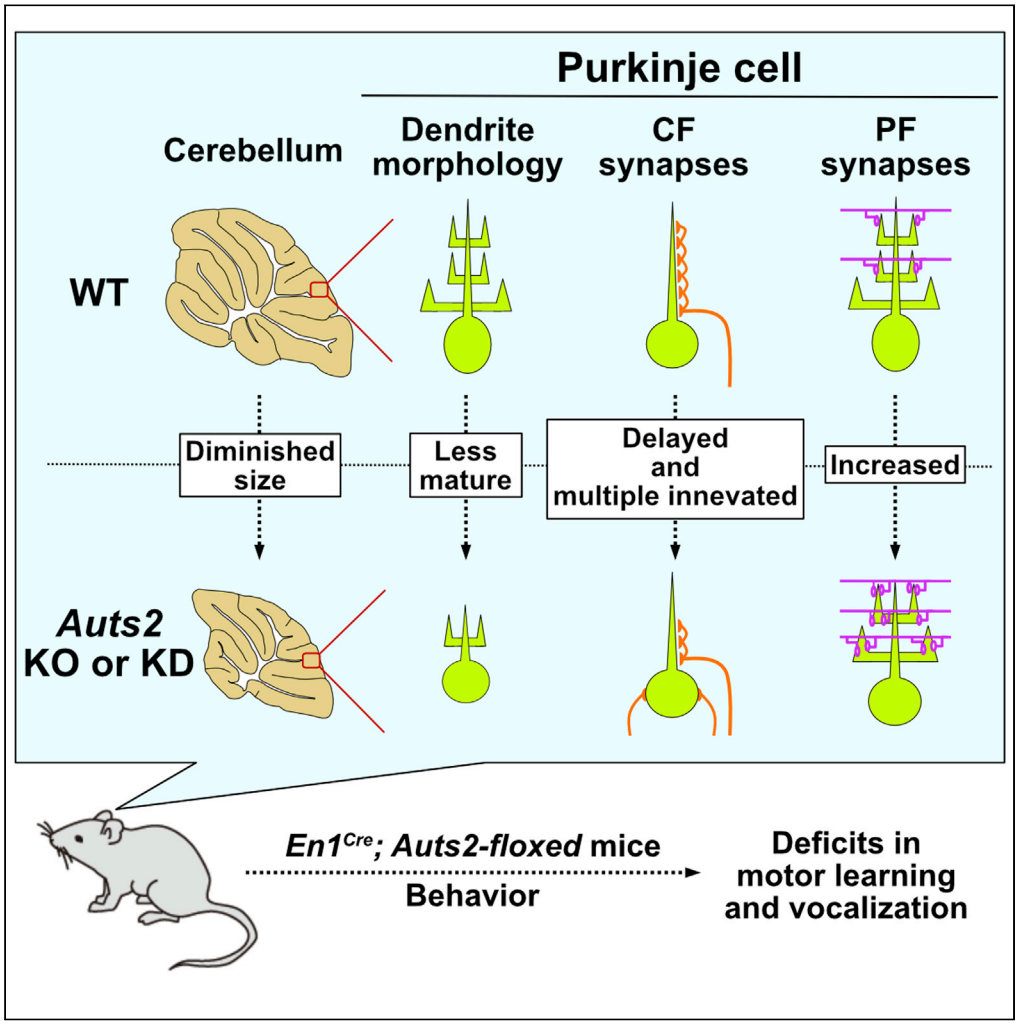

Kunihiko Yamashiro, Kei Hori, Esther S.K. Lai, ..., Naofumi Uesaka, Masanobu Kano, Mikio Hoshino

khori@ncnp.go.jp (K.H.)
hoshino@ncnp.go.jp (M.H.)

HIGHLIGHTS

Loss of *Auts2* leads to the reduction of cerebellar size

AUTS2 promotes the dendritic maturation of Purkinje cells

AUTS2 participates in PF and CF synapse development of Purkinje cells

Auts2 cKO mice exhibit the impaired motor learning and vocal communications

Yamashiro et al., iScience *23*, 101820
December 18, 2020 © 2020 The Author(s).
https://doi.org/10.1016/j.isci.2020.101820

iScience

CellPress
OPEN ACCESS

Article

AUTS2 Governs Cerebellar Development, Purkinje Cell Maturation, Motor Function and Social Communication

Kunihiko Yamashiro,[1,2] Kei Hori,[1,*] Esther S.K. Lai,[3,4] Ryo Aoki,[1,2] Kazumi Shimaoka,[1] Nariko Arimura,[1] Saki F. Egusa,[1] Asami Sakamoto,[1] Manabu Abe,[5] Kenji Sakimura,[5] Takaki Watanabe,[4] Naofumi Uesaka,[4,6] Masanobu Kano,[4] and Mikio Hoshino[1,2,7,*]

SUMMARY

***Autism susceptibility candidate 2* (*AUTS2*), a risk gene for autism spectrum disorders (ASDs), is implicated in telencephalon development. Because AUTS2 is also expressed in the cerebellum where defects have been linked to ASDs, we investigated AUTS2 functions in the cerebellum. AUTS2 is specifically localized in Purkinje cells (PCs) and Golgi cells during postnatal development. *Auts2* conditional knockout (cKO) mice exhibited smaller and deformed cerebella containing immature-shaped PCs with reduced expression of *Cacna1a*. *Auts2* cKO and knock-down experiments implicated AUTS2 participation in elimination and translocation of climbing fiber synapses and restriction of parallel fiber synapse numbers. *Auts2* cKO mice exhibited behavioral impairments in motor learning and vocal communications. Because *Cacna1a* is known to regulate synapse development in PCs, it suggests that AUTS2 is required for PC maturation to elicit normal development of PC synapses and thus the impairment of *AUTS2* may cause cerebellar dysfunction related to psychiatric illnesses such as ASDs.**

INTRODUCTION

The cerebellum is a well-defined brain region known to control motor coordination and function. The cerebellar cortex consists of a uniform three-layered structure: the molecular layer (ML), Purkinje cell layer (PCL), and granule cell layer (GCL) (Ito, 2006). Because its highly stereotyped cytoarchitecture is composed of fewer types of neuronal cells compared with other brain regions, the cerebellum has been used as a good model system to study neurogenesis and cell morphogenesis as well as circuit assembly (Sillitoe and Joyner, 2007). Among neurons in the cerebellar cortex, Purkinje cells (PCs) are the sole output neurons that extend a long axon to deep cerebellar nuclei (DCN) neurons (White and Sillitoe, 2013). In mouse brains, PCs are generated at the ventricular zone of the cerebellar primordia during embryonic (E) 11–13 days and then migrate and differentiate until birth (Altman and Bayer, 1978; Yuasa et al., 1991). During the first three weeks of postnatal development, PCs form apical stem dendrites with extremely elaborated branches. Each PC receives excitatory presynaptic inputs from a single climbing fiber (CF) originating from a neuron in the inferior olivary nucleus (ION) and simultaneously accepts inputs from the multiple parallel fibers (PFs) projecting from granule cells (GCs). Accumulating evidence demonstrates that the cerebellum is increasingly appreciated as a potential regulator for high-order brain functions. Functional magnetic resonance imaging (fMRI) studies on human subjects have revealed that the activation of the cerebellum is associated with social cognition and emotional processing (Schmahmann and Caplan, 2006; Van Overwalle et al., 2014). Accordingly, isolated cerebellar injury or cerebellar lesions have been linked to various types of cognitive and social impairments (Limperopoulos et al., 2007; Schmahmann and Sherman, 1998). Postmortem studies in individuals with autism spectrum disorders (ASDs) displayed cerebellar PC loss (Amaral et al., 2008; Bauman and Kemper, 2005). In addition, animal models of various neurological disorders revealed that a reduction in the number or dysfunction of PCs leads to abnormal social behaviors (Tsai et al., 2012). However, despite the significance of proper development and function of PCs for socio-cognitive processes in the cerebellum, the pathological mechanisms underlying how impairments of development or function of PCs contribute to neurological disorders remain to be clarified.

[1]Department of Biochemistry and Cellular Biology, National Institute of Neuroscience, National Center of Neurology and Psychiatry (NCNP), Tokyo 187-8502, Japan

[2]Department of NCNP Brain Physiology and Pathology, Graduate School of Medical and Dental Sciences, Tokyo Medical and Dental University, Tokyo 113-8510, Japan

[3]Brain Mechanism for Behavior Unit, Okinawa Institute of Science and Technology Graduate University, Okinawa 904-0495, Japan

[4]Department of Neurophysiology, Graduate School of Medicine, The University of Tokyo, Tokyo 113-0033, Japan

[5]Department of Animal Model Development, Brain Research Institute, Niigata University, Niigata 951-8585, Japan

[6]Department of Cognitive Neurobiology, Graduate School of Medical and Dental Sciences, Tokyo Medical and Dental University, Tokyo 113-8510, Japan

[7]Lead Contact

*Correspondence: khori@ncnp.go.jp (K.H.), hoshino@ncnp.go.jp (M.H.)

https://doi.org/10.1016/j.isci.2020.101820

This is an open access article under the CC BY license (http://creativecommons.org/licenses/by/4.0/).

Autism susceptibility candidate 2 (*AUTS2*) (also termed "activator of transcription and developmental regulator") has been identified in human genetic studies as a risk gene for numerous types of psychiatric illnesses, including ASDs, intellectual disabilities (IDs), and schizophrenia (Hori and Hoshino, 2017; Oksenberg and Ahituv, 2013). In addition, the genomic structural variants in the *AUTS2* locus have been associated with multiple types of neurological disorders such as attention deficit hyperactivity disorder (ADHD) and dyslexia (Elia et al., 2010; Girirajan et al., 2011). Moreover, *AUTS2* has been implicated in other neuropathological conditions such as epilepsy, motor delay, and language delay (Mefford et al., 2010; Sengun et al., 2016; Talkowski et al., 2012). *Auts2* is a long and complex gene, and it has been suggested that various isoforms are produced by alternative (splicing and alternative) transcriptional start sites. They have been intensively analyzed in zebrafish (Kondrychyn et al., 2017) but have not yet been reported in great detail in mammals. The human *AUTS2* gene has two main transcripts, a full-length and a 3′ short transcript with an alternative transcription start site within exon 9 (Beunders et al., 2013), whereas mouse *Auts2* has a full-length and two 3′ short isoforms arising from exon 8 and 9 (Hori and Hoshino, 2017). In the developing mouse brain, AUTS2 is highly expressed in various brain regions including cerebral cortex, hippocampus, and cerebellum (Bedogni et al., 2010). The knockdown of zebrafish *auts2* by morpholino leads to the drastic reduction of brain size, especially in caudal regions including the midbrain and hindbrain as well as the cerebellum (Oksenberg et al., 2013), suggesting that AUTS2 is crucial for brain tissue development. We have previously reported that cytoplasmic AUTS2 regulates actin cytoskeletal rearrangements via Rho family small GTPases, Rac1 and Cdc42, to control neuronal migration and neurite formation in the cortical neurons of prenatal forebrains (Hori and Hoshino, 2017). In addition, another group showed that nuclear AUTS2 interacts with histone modifiers such as Polycomb group (PcG) protein complex PRC1 and histone acetyltransferase P300 and acts as a transcriptional activator (Gao et al., 2014). Moreover, we previously showed that AUTS2 restricts the number of excitatory synapses without affecting that of inhibitory synapses in the telencephalon (Hori et al., 2020). This function is elicited by nuclear AUTS2, because nuclear localizing, but not cytoplasmic-localizing, AUTS2 is able to rescue the corresponding synaptic abnormalities in the *Auts2*-knockdowned primary cultured hippocampal neurons.

In the cerebellar cortex, the expression of *Auts2* mRNA was reported to start in PCs from the early neurodevelopmental stages and is maintained through postnatal and adult stages (Bedogni et al., 2010). However, little is known with regard to the physiological roles of AUTS2 in PC development due to lack of studies on the consequences of *Auts2* gene deletion in the cerebellum. Moreover, the extent of AUTS2 contribution to the pathogenesis of psychiatric disorders associated with the cerebellum remains unclear. Because conventional homozygous *Auts2* knockout mice are neonatal lethal (Hori et al., 2014), it has been difficult to study the function of AUTS2 in the cerebellum at postnatal stages and adulthood.

In this study, we generated *Auts2* conditional knockout (cKO) mice by crossing $Auts2^{flox}$ mice with $En1^{Cre}$ mice to disrupt the *Auts2* locus in the cerebellum (Hori et al., 2014; Kimmel et al., 2000; Sgaier et al., 2007). In the cerebella of these cKO mice, exon 8 of the *Auts2* gene is deleted by the Cre recombinase activity, leading to the complete elimination of both full-length AUTS2 (~170 kDa) as well as the C-terminal AUTS2 short isoform variant 1 (S-AUTS2-Var1; ~88 kDa). In contrast, the C-terminal AUTS2 short isoform variant 2 (S-AUTS2-Var2; ~78 kDa) that originates from exon 9 is aberrantly increased, as has been observed in the cerebral cortex of *Auts2* global KO mice (Hori et al., 2014). *Auts2* cKO mice displayed drastic reduction of cerebellar size accompanied with reduced PC number. The maturation of PCs was delayed in *Auts2* cKO mice, in terms of dendrite morphology and gene expression profile. Although CF synapse development was impaired in the *Auts2* cKO mice, excessive PF synapse formation was observed. Furthermore, *Auts2* cKO mice exhibited abnormal motor function and vocal communication behavior. Thus, these findings suggest that *Auts2* is involved in the maturation and synaptogenesis of PCs during cerebellar development, contributing to vocal communication as well as motor function. Because vocal communication deficits were also observed in heterozygous *Auts2* cKO mice, this study should provide insight into understanding the pathology of human psychiatric disorders with *AUTS2* mutations, which are in general, heterozygous.

RESULTS

AUTS2 Is Specifically Expressed in Purkinje Cells and Golgi Cells in the Postnatal Cerebellar Cortex

To investigate the role of AUTS2 in postnatal cerebellar development, we examined the expression of AUTS2 in the cerebellum. Our previous study revealed that AUTS2 isoforms including the full-length

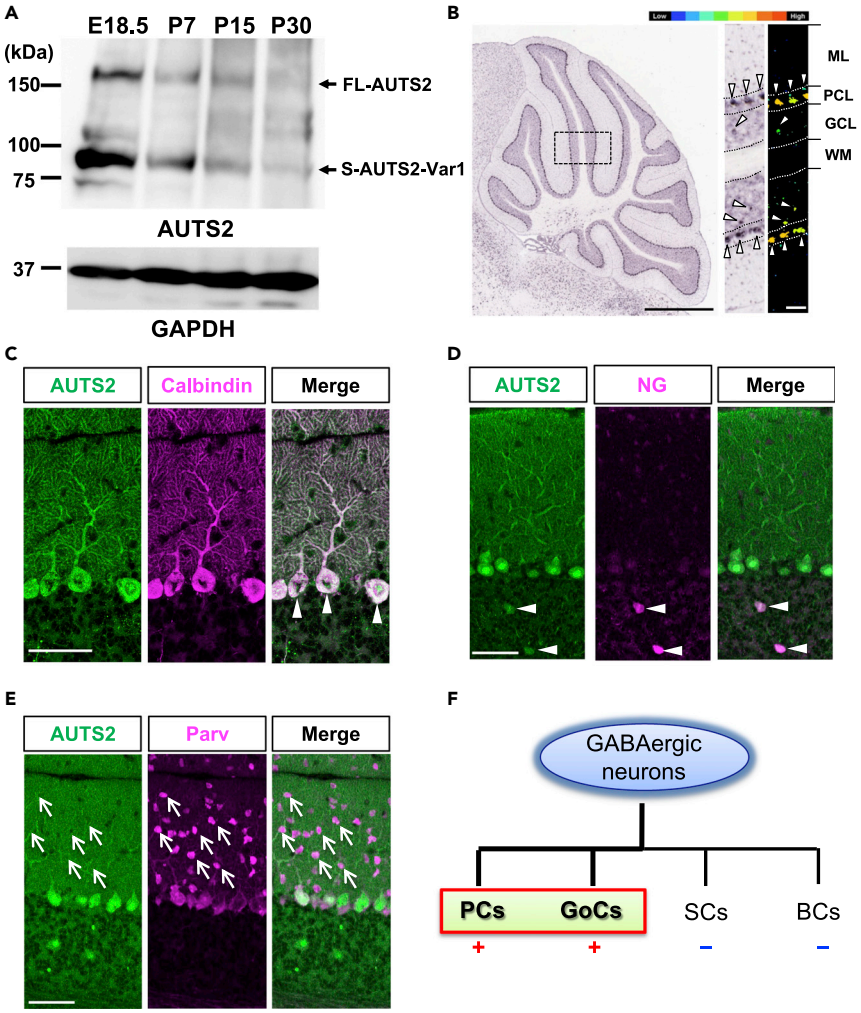

Figure 1. AUTS2 Expression in the Inhibitory Neurons in the Cerebellar Cortex

(A) Expression of AUTS2 in the developing cerebellum. Arrows indicate the full-length (FL-AUTS2) or C-terminal short isoform variant 1 (S-AUTS2-Var1) of AUTS2 protein.

(B) *In situ* hybridization for *Auts2* in P56 cerebellum (adapted from the Allen Brain Atlas, experiment #79904156). Arrowheads indicate the expression of *Auts2* mRNA. ML: Molecular layer, PCL: Purkinje cell layer, GCL: Granule cell layer, WM: White matter. Scale bar, 1 mm (left panel) and 100 μm (right panel).

(C–E) Co-immunostaining of AUTS2 with inhibitory neuronal markers Calbindin (Purkinje cells), Neurogranin (NG; Golgi cells), and Parvalbumin (Parv; interneurons including stellate cells and basket cells at ML and Purkinje cells) in P25 cerebellar cortex. AUTS2 is expressed in Purkinje cells and Golgi cells (arrowheads in C and D), whereas there are no detectable signals in the molecular layer interneurons (arrows in E). Scale bars, 50 μm.

(F) Summary diagram of AUTS2^{+} cells in inhibitory neurons in cerebellar cortex. PCs: Purkinje cells, GoCs: Golgi cells, SCs: stellate cells, BCs: basket cells.

See also Figure S1.

(FL)-AUTS2 protein as well as the C-terminal short isoform variant 1 (S-AUTS2-Var1) are expressed in the cerebral cortex (Hori et al., 2014). Western blotting analysis with whole cerebellar lysates showed that FL-AUTS2 and S-AUTS2-Var1 are expressed at the late embryonic stage (E18.5), and expression gradually decreases throughout postnatal development, although still observed at postnatal day 30 (P30) (Figure 1A). Consistent with previous studies (Bedogni et al., 2010), *in situ* hybridization data from the Allen Brain Atlas (http://portal.brain-map.org) show that *Auts2* is highly expressed in PCs in adults (Figure 1B). In addition, we found that *Auts2* mRNA is also detected in certain cells in the granule cell layer (GCL) (Arrowheads in Figure 1B). Co-immunostaining of adult cerebellar tissues using the anti-AUTS2 antibody with cell-specific markers demonstrated that AUTS2 colocalized with calbindin, a marker for PCs (Figure 1C). Furthermore,

immunofluorescence analyses on the developing cerebellar tissue sections postnatally revealed intense AUTS2 immunosignals in PCs equivalent to those observed in adult cerebellum (Figure S1), indicating that AUTS2 expression is maintained in PCs in development and adulthood. Within the PCs, AUTS2 is found in cell bodies including nuclei and dendrites (Figures 1C and S1). Consistent with *Auts2* mRNA expression, the immuno-signals for AUTS2 were also detected in the neurogranin-positive Golgi cells in the GCL (Figure 1D) (Singec et al., 2003). In contrast, AUTS2 was not detected in the parvalbumin-positive interneurons in the ML including stellate cells and basket cells (Figure 1E). These results suggest that AUTS2 is exclusively expressed in PCs and Golgi cells in the cerebellar cortex during postnatal development (Figure 1F).

Auts2 Conditional Knockout Mice Exhibit Defects in Cerebellar Development

We previously reported that homozygotes for the loss of function allele ($Auts2^{del8}$) were neonatally lethal (Hori et al., 2014). To better understand the roles for AUTS2 in postnatal cerebellar development, we generated *Auts2* conditional KO (cKO) mice by crossing $Auts2^{flox}$ with $En1^{Cre}$ mice, in which exon 8 of *Auts2* can be specifically ablated in the rhombomere-1-derived brain area including the cerebellum from the mid-embryonic stages (E9.5~) (Figure 2A) (Kimmel et al., 2000; Sgaier et al., 2007). In this study, we analyzed the $En1^{Cre/+}$;$Auts2^{flox/flox}$ (homozygous *Auts2* cKO) and $Auts2^{flox/flox}$ (control) mice unless otherwise noted. As previously observed in the cerebral cortices of $Auts2^{del8}$ mutants (Hori et al., 2014), immunoblotting of cerebellar tissue extracts confirmed that in the *Auts2* cKO cerebella, both FL-AUTS2 and S-AUTS2-Var1 are eliminated, whereas S-AUTS2-Var2 that originates from exon 9 is abnormally increased (Figure 2B). To confirm the specificity of the AUTS2 antibody used in immunoblotting, we performed immunostaining using this antibody on prenatal cerebellum prepared from $Auts2^{neo/neo}$ homozygous mutant mice, in which all AUTS2 isoforms were almost completely eliminated (Figure S2) (Hori et al., 2014). Immunofluorescence shows the expression of AUTS2 in RORα-positive Purkinje cells in WT cerebellum, whereas immuno-signals were almost completely absent in $Auts2^{neo/neo}$ homozygotes (Figure S2), indicating the high specificity of this antibody for AUTS2. Moreover, quantitative PCR showed that excision of exon 8 within the *Auts2* mRNA was almost complete in the cerebella of *En1-Cre;* $Auts2^{flox/flox}$, whereas exon 8 remained intact in the cerebral cortices of the same animals (Figure S3).

Auts2 cKO mutants were viable but had a significant reduction in body weight or exhibited developmental delays (Figure 2C). At P30, cerebella isolated from the *Auts2* cKO mice were smaller than those of controls (Figure 2D). Sagittal cerebellar sections of *Auts2* cKO mice revealed a dramatic reduction in size of both hemispheres and vermis regions compared with control (Figure 2D). In addition, *Auts2* cKO mutants exhibited aberrant cerebellar cortical morphologies. Several lobules including lobe X, Crus I, and copula pyramidis were severely reduced in size or absent (Figure 2D). Sections of *Auts2* cKO cerebellar cortices revealed that although the basic laminar structure consisting of ML-PCL-GCL was normal (Figure 2D), the total areas including both ML and GCL were decreased by ~56% (Figure 2E). Furthermore, the number of PCs in *Auts2* cKO mice were significantly decreased, whereas the density of PCs was similar (Figures 2F and S4).

In addition to the cerebellum, *En1* is expressed in the caudal midbrain (Sgaier et al., 2007). Although there are no gross histological differences in the midbrain regions between *Auts2* cKO mice and controls (data not shown), we found that the number of dopaminergic midbrain neurons in the substantia nigra were slightly but significantly reduced in *Auts2* cKO mice compared with the control mice (Figure S5).

It is well established that the signaling factor Sonic Hedgehog (SHH), secreted from PCs, plays a key role for GC expansion during the cerebellar development (Dahmane and Ruiz i Altaba, 1999). To determine whether loss of *Auts2* leads to reduced SHH expression or impairment of SHH signaling in the developing cerebellum, we performed immunostaining for SHH and its downstream effector GLI1 on tissue sections from the developing cerebellum. Immunofluorescence on cerebellum from *Auts2* cKO mice at P7 showed that the SHH immunosignals in PCs were comparable with control (Figure S6A). We also detected the expression of GLI1 in the external granular layer (EGL) in both genotypes, suggesting that SHH signaling functions normally to activate the expression of the SHH downstream effector(s) in granule neuron precursors in the *Auts2* cKO cerebellum (Figure S6A). Furthermore, RT-qPCR analysis revealed no significant differences in the expression levels of these genes per cerebellar unit among the genotypes (Figure S6B). These results imply that the reduction of GCs in the *Auts2* mutants might be attributed to the reduction of SHH due to the diminished number of PCs. Taken together, these results suggest that AUTS2 is critical for cerebellar development.

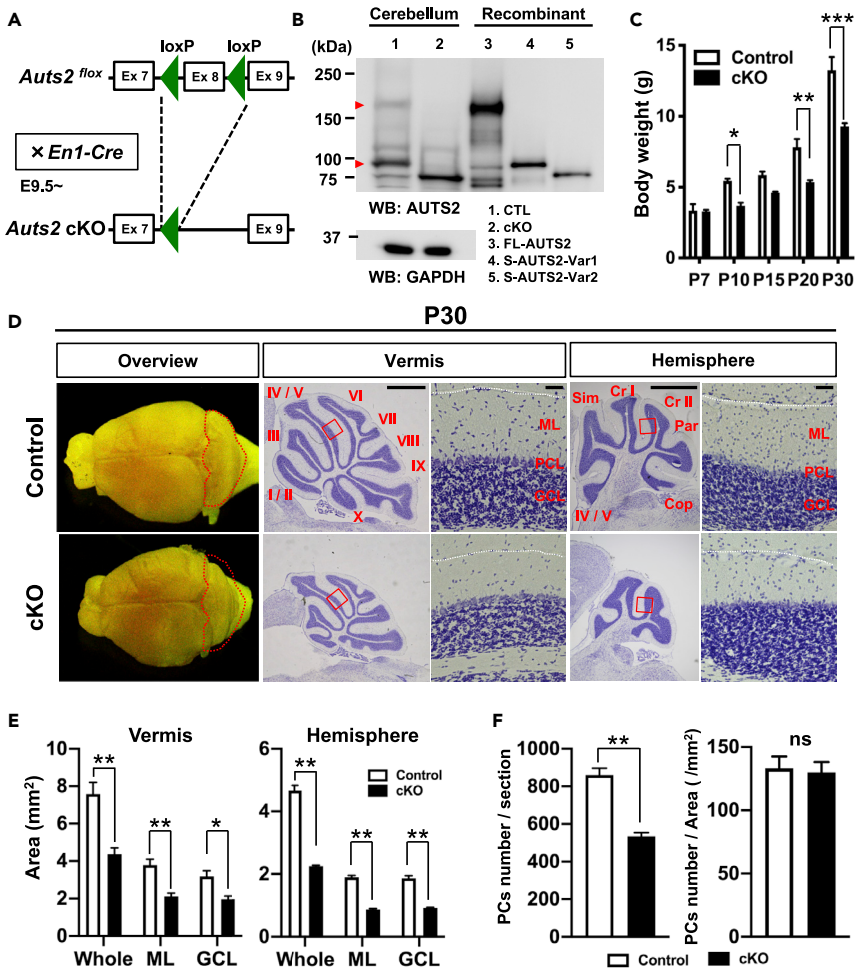

Figure 2. Cerebellar Hypoplasia in *Auts2* Conditional Knockout Mice

(A) Schematics of the targeting strategy for *Auts2* conditional knockout (*Auts2* cKO) mice. Exon 8 of *Auts2* gene was conditionally deleted by crossing *Auts2-floxed* mice with *Engrailed-1*$^{Cre/+}$ (*En1*$^{Cre/+}$) mice.

(B) Immunoblot for AUTS2 proteins in cerebellar lysates from *Auts2* $^{flox/flox}$ (Control; CTL) and *En1*$^{Cre/+}$;*Auts2* $^{flox/flox}$ homozygotic cKO mice at P0. Immunoblot of lysates from HEK293T cells expressing the recombinant full-length AUTS2 (FL-AUTS2) and the C-terminal AUTS2 short variants (S-AUTS2-Var1 and Var2) are also shown. Full-length AUTS2 as well as the S-AUTS2-Var1 were completely eliminated in *Auts2* cKO homozygotic mutant cerebellum (red arrowheads), whereas the S-AUTS2-Var2 was alternatively increased.

(C) Plot of body weights in control and *Auts2* cKO mice from P7 to P30. n = 2–7 mice.

(D) Whole-mount images and Nissl-stained parasagittal sections in control and *Auts2* cKO mice at P30. The folia of vermis and hemisphere are indicated as roman numerals (I-X) and abbreviations (Sim: Simple lobule, Cr I and II: Crus I and II, Par: Paramedian lobule, Cop: Copula pyramidis). Higher magnification images of the boxed regions showing ML-PCL-GCL laminar structure. ML: Molecular layer, PCL: Purkinje cell layer, GCL: Granule cell layer. Scale bar, 1 mm and 50 μm.

(E) Quantification of cerebellar areas including whole, molecular layer (ML), granule cell layer (GCL) in parasagittal sections of control and *Auts2* cKO mice at P30. n = 6 slices from 3 mice.

(F) The number of PCs was decreased in the cerebellar vermis of *Auts2* cKO at P30 compared with the control, but the density of PCs was normal. n = 5 slices from 5 mice.

Data are shown as mean ± SEM. *p < 0.05, **p < 0.01, ***p < 0.001 by two-way ANOVA followed by Bonferroni's multiple comparisons test in (C), Mann-Whitney test in (E and F).

See also Figures S2–S6.

AUTS2 Regulates Dendritic Outgrowth of Purkinje Cells

Among the AUTS2-positive cerebellar inhibitory neurons, PCs play a key role in the output of processed information and control of motor function. We therefore decided to focus on the roles of AUTS2 in PC development. In the P0 cerebellar cortex, postmigratory PCs initially display "fusiform" morphology with

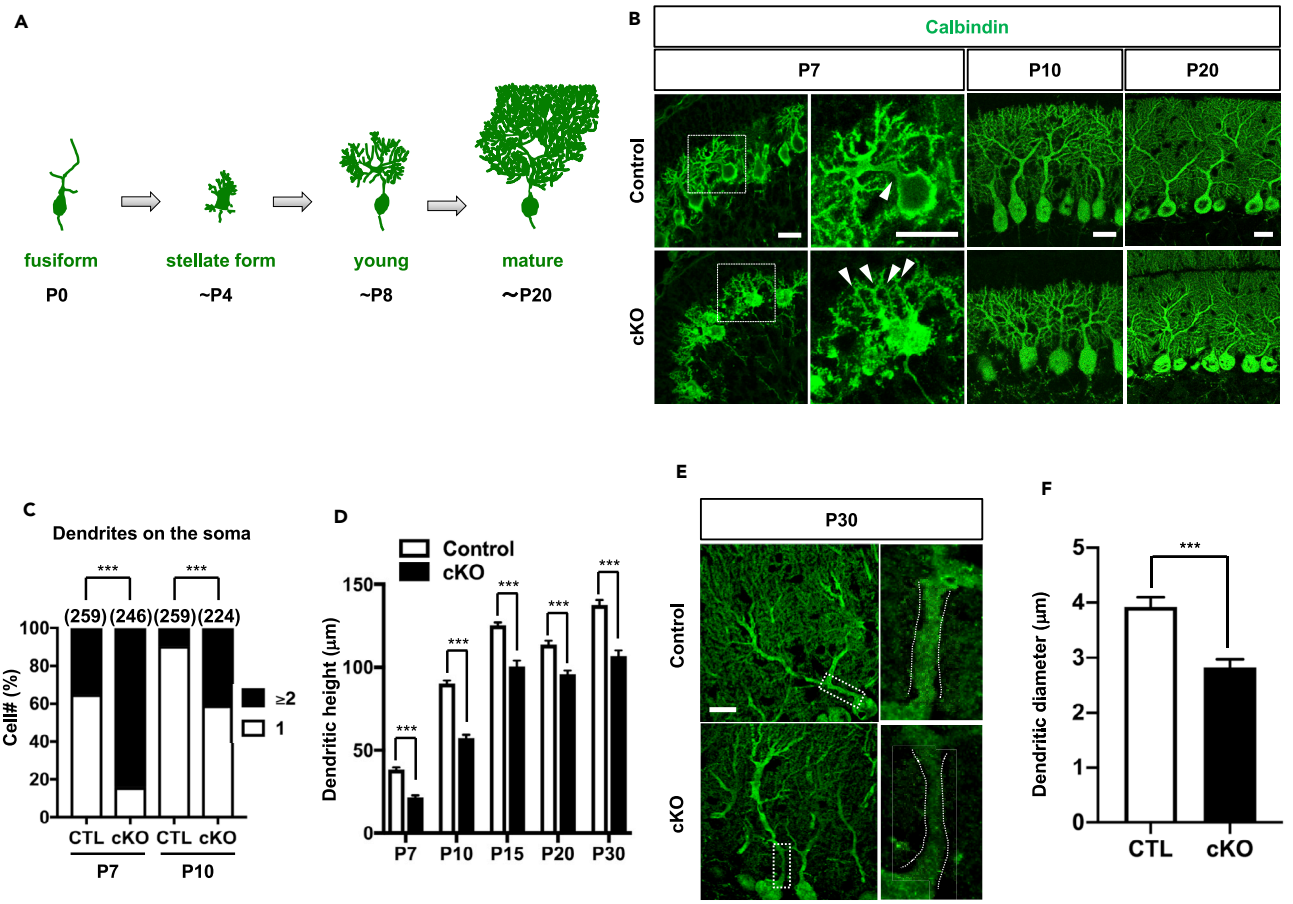

Figure 3. Loss of *Auts2* Induces Impaired Maturation of PCs

(A) Schematics of PC morphology during the postnatal development.

(B) Representative immunofluorescent images of Calbindin-positive PCs in lobule IV/V from P7 to P20 in control (upper panels) and *Auts2* cKO mice (lower panels). Arrowheads indicate dendrites on the soma. Scale bars, 20 μm.

(C) Proportion of the number of primary dendrites formed on single PC soma in lobule IV/V at P7 and P10 in control (CTL) and *Auts2* cKO mice. n = 259 cells from 3 mice at P7 and P10 for control mice, and n = 246 cells from 3 mice at P7, n = 224 cells from 3 mice at P10 for *Auts2* cKO mice.

(D) Measurement of dendrite lengths of PCs in lobule IV/V toward the pia surface during postnatal development. n = 12–15 cells from 3 mice for control and *Auts2* cKO mice.

(E) Representative images of primary dendritic shafts of PCs in lobule IV/V labeled with Calbindin at P30 in control and *Auts2* cKO mice. Scale bar, 20 μm.

(F) Reduced PC primary dendrite thickness of lobule IV/V in *Auts2* cKO mice. n = 12–14 cells from 3 mice. Data are shown as mean ± SEM. *p < 0.05, **p < 0.01, ***p < 0.001 by Chi-squared test in (C), two-way ANOVA followed by Bonferroni's multiple comparisons test in (D), Mann-Whitney test in (F).

See also Figure S7.

a few primitive apical dendrites (Figure 3A). They then transform into "stellate cells" by retracting primitive dendrites, which in turn, form multiple disoriented perisomatic dendrites by P4. During the next four days, these irregular dendrites are progressively regressed concomitantly with the occurrence of single stem apical dendrite (primary dendrite), and PCs enter the "young PC" stage by P8. Subsequently, PCs continue to extend dendrites and form highly refined branches, reaching maximal lengths by around P20 (Sotelo and Dusart, 2009). To investigate the dendritogenesis of PCs in *Auts2* cKO mice, we used calbindin. In the control cerebellar cortex at P7, the majority of PCs displayed typical "young PC"-like morphology, with a single thick stem dendrite and elaborated branches (Figures 3B and 3C). In contrast, most of the PCs in *Auts2* cKO mice at the same age appeared stellate cell-like in shape with more than 2 perisomatic dendrites (Figures 3B and 3C). By P10, although the proportion of the cells with young PC morphologies was increased to ~60% in *Auts2* cKO mice, higher numbers of PCs still exhibited stellate-like shapes compared with the controls (Figures 3B and 3C). These observations suggest that the pruning process of PC dendrites is impaired in *Auts2* cKO mice. Consistent with a reduction in the ML in *Auts2* cKO cerebellum (Figure 2E), we observed a reduction in dendritic outgrowth of PCs in *Auts2* cKO cerebellum throughout postnatal stages

(Figure 3D). The diameter of the first segment of primary dendrites was significantly smaller in *Auts2* cKO PCs than that of control (Figures 3E and 3F).

We further examined whether the impairments in dendrite development of PCs in *Auts2* cerebellum is caused by the increased S-AUTS2-Var2 expression. Overexpression of S-AUTS2-Var2 in PCs in WT cerebellum did not, however, affect dendritic outgrowth nor its morphology (Figure S7), suggesting that the defects in dendritogenesis in *Auts2* cKO mutant PCs was not due to a gain-of function effect by increased S-AUTS2-Var2. Taken together, these results suggest that AUTS2 is involved in proper development of PC dendrites.

Loss of *Auts2* Causes Abnormal CF and PF Synapse Formation in PCs

We next investigated the function of AUTS2 in PC synapse formation. PCs receive excitatory synaptic inputs from CF neurons in the ION. The CF axon terminals from ION translocate upward from soma to primary dendrites of PCs, forming excitatory synapses (CF synapses). Immunohistochemistry of postnatal cerebellar sections with VGlut2, a marker for presynaptic terminals of the CFs, showed that, at P15, VGlut2-puncta traversed 70.45 $\pm$ 1.54% of the ML thickness in control cerebella, whereas they were found only in the deeper regions (35.93 $\pm$ 3.01%) of the ML in the *Auts2* cKO cerebella (Figures 4A and 4B). Although those VGlut2-puncta gradually translocated upward in the *Auts2* cKO cerebella as development proceeded, they never reached the level of the control mice at P30 (Figures 4A and 4B). Similarly, VGlut2-puncta in the ML at *Auts2* cKO cerebella were significantly decreased compared with the controls (Figures S8A and S8B). This suggests that development of CF synapses, particularly their translocation process, is delayed in *Auts2* cKO mice.

We next assessed the parallel fiber (PF) synapses by immunostaining with GluD2, a molecular marker for PF synapses in PC dendrites (Yamasaki et al., 2011). In contrast to the CF synapses, we observed that loss of *Auts2* resulted in an increase of the GluD2-immunoreactivities in the ML of *Auts2* cKO mice compared with those of control mice at P15 and P30 (Figures 4C and 4D). Likewise, high-magnification images in the ML showed that the density of GluD2-puncta was significantly higher in *Auts2* cKO mice (Figures S8C and S8D), suggesting that loss of *Auts2* leads to excessive PF synapse formation. Golgi staining also revealed that the dendritic spine density at the distal end of the PC dendrites was significantly increased in *Auts2* cKO mutants compared with controls at P16 and P30 (Figures 4E and 4F). Because the distal part of PC dendrites is predominantly occupied by PF synapses (Altman, 1972), the increased number of synapses in the *Auts2* cKO cerebella were regarded as PF synapses. These findings suggest that *Auts2* is required for normal development of CF synapses, while restricting the number of PF synapses. We confirmed that overexpression of S-AUTS2-Var2 in the PCs in WT cerebellum did not alter the translocation of CF synapses (Figure S9) as well as the number of dendritic spines at the distal end of PC dendrites (Figure S10), suggesting that the aberrant excitatory synapse development observed in *Auts2* cKO mutants is caused by loss of function of AUTS2.

It was previously reported that AUTS2 acts as a transcriptional regulator for neural development (Gao et al., 2014). Furthermore, our previous RNA-seq analysis showed that disruption of *Auts2* in mouse forebrains resulted in changes in global expression of genes associated with multiple aspects of neurodevelopment, including dendrite morphogenesis and synapse development (Hori et al., 2020). Quantitative PCR analysis showed no significant changes in the expression levels of *RORα* (Figure S11A) (Takeo et al., 2015). Meanwhile, we observed the downregulation of *Cacna1a*, which reportedly regulates the excitatory synapse formation in PCs, in the *Auts2* cKO mice (Figure S11A) (Hashimoto et al., 2011; Miyazaki et al., 2004, 2012). Furthermore, we verified that the intensity of CaV2.1 (a product of *Cacna1a* gene) immunostaining, is markedly reduced in *Auts2* cKO PCs (Figures S11B and S11C). These results imply that AUTS2 may be involved in CF and PF synapse development by regulating the expression of synaptic genes, such as *Cacna1a*.

Purkinje-Cell-Specific *Auts2* Knockdown Impairs Excitatory Synapse Functions

Next, we performed an electrophysiological analysis to investigate the loss-of-function effects of *Auts2* on PCs of interest. To evaluate the cell-autonomous effects of *Auts2* inactivation on the synaptic transmission properties of PCs, we introduced a vector expressing EGFP and *Auts2*-targeted microRNA (miRNA) driven by the PC-specific L7 promoter into PCs by *in utero* electroporation at E11.5-12.5 (Figure 5A). This miRNA was confirmed by western blotting to successfully downregulate the expression of both FL-AUTS2 and C-terminal short isoforms (Figure S12). Immunohistochemical analysis revealed that EGFP-positive cells

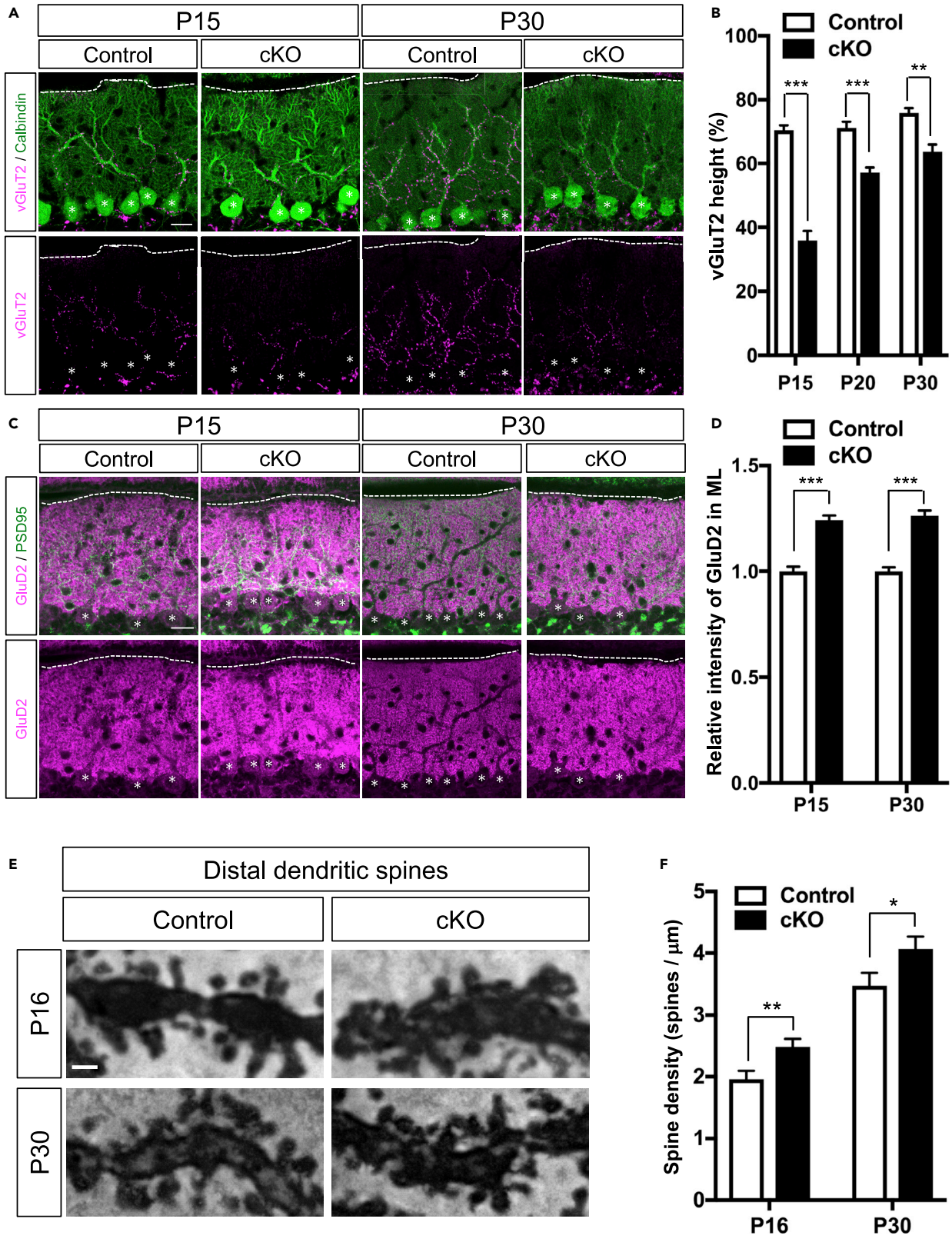
A
P15
P30
Control
cKO
Control
cKO
vGluT2 / Calbindin
vGluT2
B
Control
cKO
vGluT2 height (%)
100
80
60
40
20
0
***
***
**
P15
P20
P30
C
P15
P30
Control
cKO
Control
cKO
GluD2 / PSD95
GluD2
D
Control
cKO
Relative intensity of GluD2 in ML
1.5
1.0
0.5
0.0
***
***
P15
P30
E
Distal dendritic spines
Control
cKO
P16
P30
F
Control
cKO
Spine density (spines / µm)
5
4
3
2
1
0
**
*
P16
P30

Figure 4. Delayed CF Translocation and Excessive PF Formation in *Auts2* Conditional Knockout Mice

(A) Double immunostaining with calbindin (green) and climbing fiber (CF) synaptic marker VGlut2 (magenta) on the cerebellar lobule IV/V of control and *Auts2* cKO mice at P15 and P30. Scale bars, 20 μm.

(B) Quantitative analysis of the ratio of VGlut2 height to the tip of PC dendrites of lobule IV/V in control and *Auts2* cKO cerebellum during P15-30. n = 12–15 cells from 3 mice.

(C) Representative images of co-immunostaining with PSD-95 (green) and parallel fiber (PF) postsynaptic marker GluD2 (magenta) of lobule IV/V in the molecular layer (ML) of control and *Auts2* cKO mice at P15 and P30. Scale bars, 20 μm.

(D) Increased immunofluorescence intensity levels of GluD2 in lobule IV/V of *Auts2* cKO mice at P15 and P30. n = 72–108 areas from 3 mice.

(E) Representative images of the dendritic spines on distal PC dendrites in the Golgi-stained cerebellar lobule IV/V of control and *Auts2* cKO mice at P16 and P30. Scale bar, 1 μm.

(F) The density of distal dendritic spines on PCs of lobule IV/V was increased in *Auts2* cKO mice at P16 and P30. n = 18–27 branches, 3 mice.

Data are shown as mean ± SEM. *$p < 0.05$, **$p < 0.01$, ***$p < 0.001$ by two-way ANOVA followed by Bonferroni's multiple comparisons test in (B), Mann-Whitney test or unpaired Student's t-test in (D and F). Dotted lines and asterisks indicate the pial surface of the ML and PC soma, respectively.

See also Figures S8–S11.

were co-labeled with the PC marker, Car8 (Figure 5B) (Patrizi et al., 2008). We subsequently performed whole-cell patch-clamp recordings in EGFP-positive or -negative PCs from acute cerebellar slices at P20-30. To examine the basic properties of overall synaptic function in PCs targeted with the *Auts2*-knockdown (KD) vector, we measured the miniature excitatory and inhibitory postsynaptic currents (mEPSCs and mIPSCs, respectively). The amplitude and frequency of mEPSCs were significantly increased in EGFP-positive *Auts2*-KD PCs compared with non-transfected PCs (EGFP-negative), whereas those of mIPSCs were not affected (Figures 5C and S13). The effect of *Auts2*-KD on mEPSCs was sufficiently restored by co-transfection of an RNAi-resistant FL-AUTS2 (*Auts2*-Res) construct, which successfully excluded off-target effects of the targeting miRNA (Figure S14). This suggests that FL-AUTS2 has the ability to regulate excitatory synaptic transmission in PCs.

Next, we recorded climbing fiber-evoked EPSCs (CF-EPSCs) to test whether loss of *Auts2* function in PCs affected CF synapse function. During early postnatal stages, each PC cell body receives multiple CF presynaptic inputs innervating from ION neurons. Subsequently, a single CF is selectively strengthened to form CF synapses, translocating along the primary dendrites of the PC while the other surplus CFs are eliminated (Kano et al., 2018). We moved the stimulation electrode systematically around the PC soma under recording and increased the stimulus intensity gradually at each stimulation site. The recording highlighted that more than 80% of PCs in WT mature cerebellum show a single-step response to an evoked CF input, indicating that the majority of PCs receive a single CF input (Figure 6A). By contrast, around half of *Auts2*-KD PCs received multiple CF inputs, compared with only 14% of non-transfected PCs (Figure 6A), indicating that loss of *Auts2* impairs the elimination of surplus CFs in PCs. We also examined the functional differentiation of multiple CF inputs by calculating two parameters, the disparity ratio and disparity index (Hashimoto and Kano, 2003). The disparity ratio and index of *Auts2*-KD PCs were similar to non-transfected PCs (Figure S15). Furthermore, we tested whether *Auts2*-KD PCs exhibited abnormal electrophysiological properties of CF-EPSCs. We observed a longer 10%–90% rise time and shorter decay time, but a normal amplitude in the total CF-EPSCs in *Auts2*-KD PCs (Table S1). Indeed, there was no difference in the extent of paired-pulse depression at inter-pulse intervals from 10 to 300 msec between *Auts2*-KD and non-transfected PCs, indicating that the release probability of CF synapses was normal in *Auts2*-KD PCs (Figure 6B). We concluded that AUTS2 is required for the selection of a single CF to innervate PC by eliminating other CFs.

Subsequently, we examined the electrophysiological properties of parallel fiber-evoked EPSCs (PF-EPSCs). The input-output curve shows that PF-EPSCs were markedly increased in *Auts2*-KD PCs (Figure 6C), consistent with the increased number of PF synapses in *Auts2* cKO mice observed by immunohistochemistry and Golgi staining (Figures 4C–4F, S8C, and S8D). Interestingly, the extent of paired-pulse facilitation was greater in *Auts2*-KD PCs, suggesting that AUTS2 is also involved in the release probability of PF synapses (Figure 6D). Taken together, these results suggest that in PCs, AUTS2 is required for the regulation of PF synaptic function.

Auts2 cKO Mice Display Motor Dysfunction and Impaired Vocal Communication

Next, we performed several behavioral analyses on *Auts2* cKO mice. In the elevated platform test (Alvarez-Saavedra et al., 2014), mice were placed on a small round elevated platform and the time for which mice remained on the platform was recorded (Figure 7A). *Auts2* cKO mice exhibited a significant decrease in

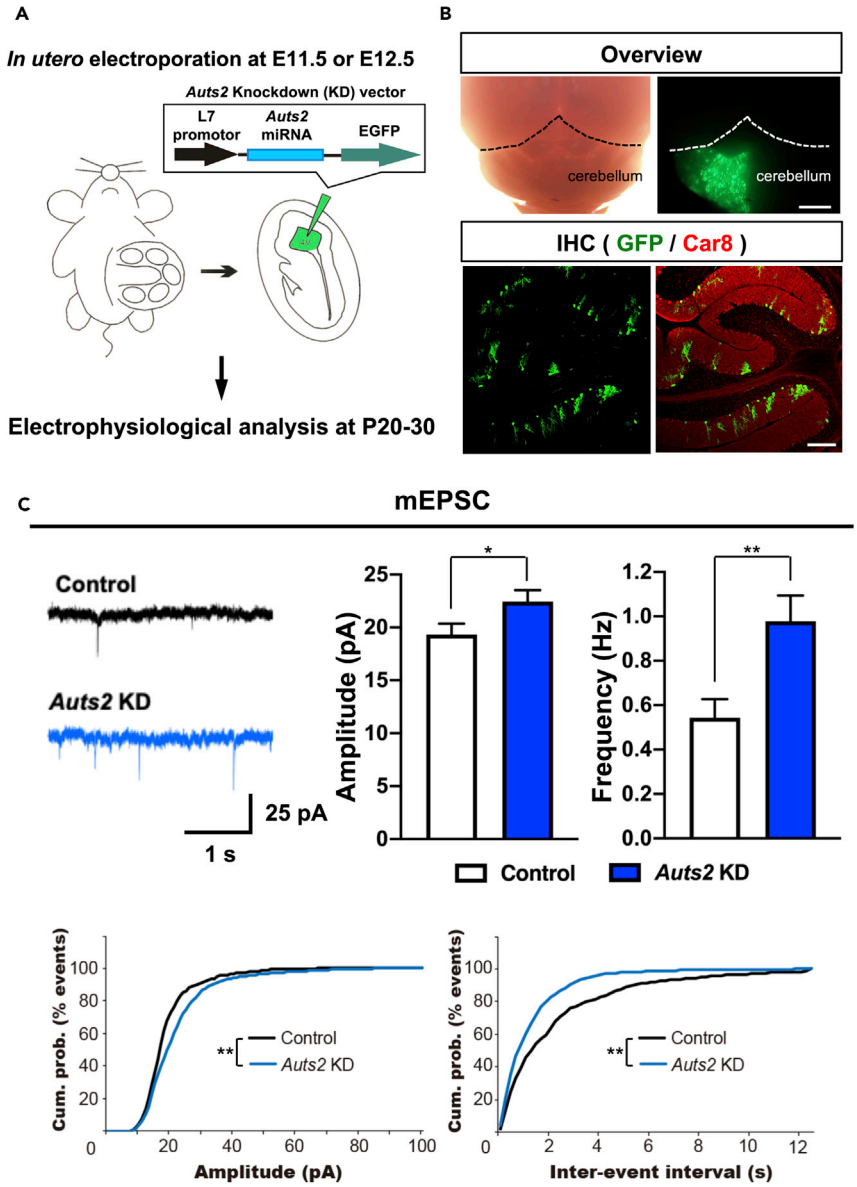

Figure 5. Knockdown of *Auts2* in PCs Exhibits Enhanced Excitatory Synaptic Transmission

(A) Schematic diagrams indicate the knockdown (KD) experiments of *Auts2* with PC-specific expression vector.

(B) Whole-mount and immunohistochemical images showing the successful introduction of *Auts2*-KD vector into PCs. EGFP-positive cells are co-labeled with a PC marker, Car8 (red). Scale bar; 1 mm (upper), 200 μm (lower).

(C) *Auts2*-KD PCs enhance amplitude and frequency of mEPSC at P20-30. Panels show representative traces (upper left) and summary graphs of the mEPSC amplitude and frequency (upper right). Bottom, cumulative probability distributions of mEPSC amplitudes (left) and inter-event interval (right) in control and *Auts2*-KD PCs. n = 11 cells, 6 mice for control and n = 13 cells, 5 mice for *Auts2* KD. Data are shown as mean ± SEM. *p < 0.05, **p < 0.01, by unpaired student t-test in bar plots, Kolmogorov-Smirnov test in cumulative frequency plots.

See also Figures S12–S14.

the length of time able to keep their balance on the platform compared with control mice, suggesting that *Auts2* cKO mice had defects in motor control (Figure 7A). We further examined the motor coordination and motor learning with the accelerating rotarod test. Control and *Auts2* cKO mice behaved similarly in the three trials during the first day of testing (Figure 7B). However, on the second day, although the motor performance of the control mice improved, *Auts2* cKO mice did not show such improvement, suggesting that *Auts2* cKO mice had abnormalities in motor learning rather than in motor coordination (Figure 7B).

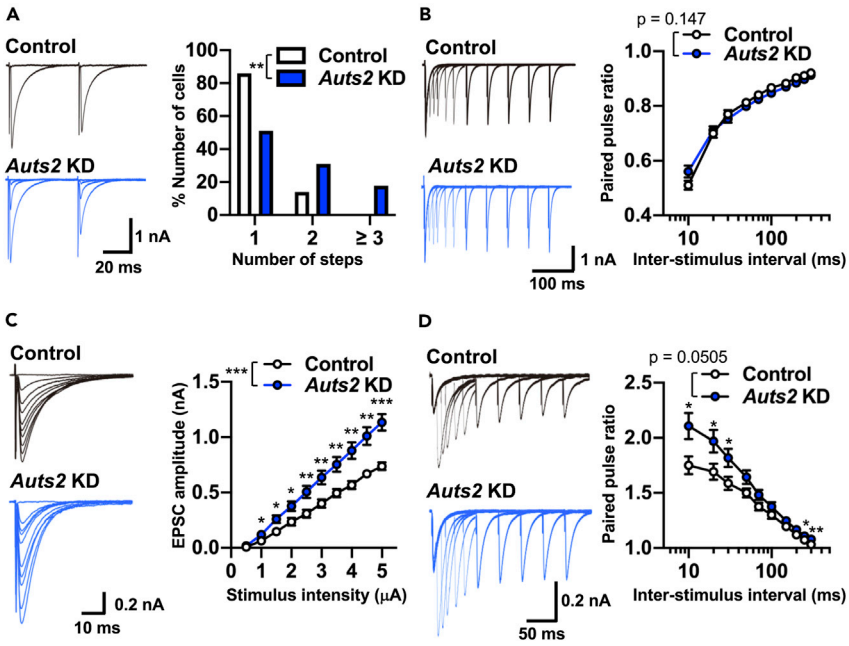

Figure 6. Knockdown of *Auts2* in PCs Impairs CF Synapse Elimination and PF Synaptic Transmission

(A) Sample traces of CF-EPSCs (left) and frequency distributions of the number of CFs innervating each PC (right) for *Auts2*-KD (blue) and control (white) PCs during P21-P30. n = 37 cells, 3 mice for control and n = 33 cells, 3 mice for *Auts2* KD.

(B) Normal paired-pulse ratio of CF-EPSCs measured at increasing inter-stimulus intervals in control and *Auts2*-KD PCs at P20-30 (left, representative traces; right, summary plots). n = 13 cells, 3 mice for control and n = 26 cells, 3 mice for *Auts2* KD.

(C) Impaired input-output relationship of PF-EPSCs in *Auts2*-KD PCs at P20-30. (left, representative traces; right, summary plots). n = 14 cells, 6 mice for control and n = 17 cells, 6 mice for *Auts2* KD.

(D) Impaired paired-pulse ratio of PF-EPSCs in *Auts2*-KD PCs at P20-30 (left, representative traces; right, summary graph). n = 13 cells, 6 mice for control and n = 16 cells, 6 mice for *Auts2* KD. Data are shown as mean ± SEM. *p < 0.05, **p < 0.01, ***p < 0.001, by Mann-Whitney U test in A, two-way ANOVA with Tukey's post hoc analysis in B-D.

See also Figure S15 and Table S1.

Subsequently, we measured ultrasonic vocalizations (USVs) of adult male mice. Male mice use courtship USVs when exposed to female mice. However, both the number and duration of calls were eliminated in homozygous *Auts2* cKO males ($En1^{Cre/+}$;$Auts2^{flox/flox}$) (Figure 7C). This suggests that AUTS2 expression in the cerebellum (or at least in the rhombomere 1 region) is critically required for male courtship USVs. Interestingly, the number and duration of calls were significantly reduced even in heterozygous *Auts2* cKO males ($En1^{Cre/+}$;$Auts2^{flox/+}$), suggesting that loss of one *Auts2* allele leads to communication deficits. This is very intriguing, because most patients with *AUTS2* mutations are heterozygotes for this gene.

DISCUSSION

In this study, we showed that specific ablation of *Auts2* in the cerebellum resulted in various structural, physiological, and behavioral abnormalities. AUTS2 has been reported to have two distinct molecular and cellular functions in neural development. We have previously reported that AUTS2 acts in cytoplasm to regulate actin cytoskeleton by controlling Rho family GTPases, such as Rac1 and Cdc42 (Hori et al., 2014). Other groups demonstrated that nuclear AUTS2 functions to regulate the transcriptional activity of genes as a component of PRC1 (Gao et al., 2014; Russo et al., 2018). Although we cannot fully conclude whether the abnormalities observed in *Auts2* cerebellar cKO mice were caused by loss of function of either cytoplasmic or nuclear AUTS2, we believe that most phenotypes, especially anatomical abnormalities including the reduced cerebellar size, delay of PC maturation as well as aberrant synapse development, might be resulted from loss of nuclear function of AUTS2, by the reasons described below. However, because cytoplasmic AUTS2 can also regulate the cellular morphology via cytoskeletal rearrangements (Hori et al., 2014), it may be possible that abnormal dendrite shapes, at least in part, are caused by loss of cytoplasmic AUTS2 function.

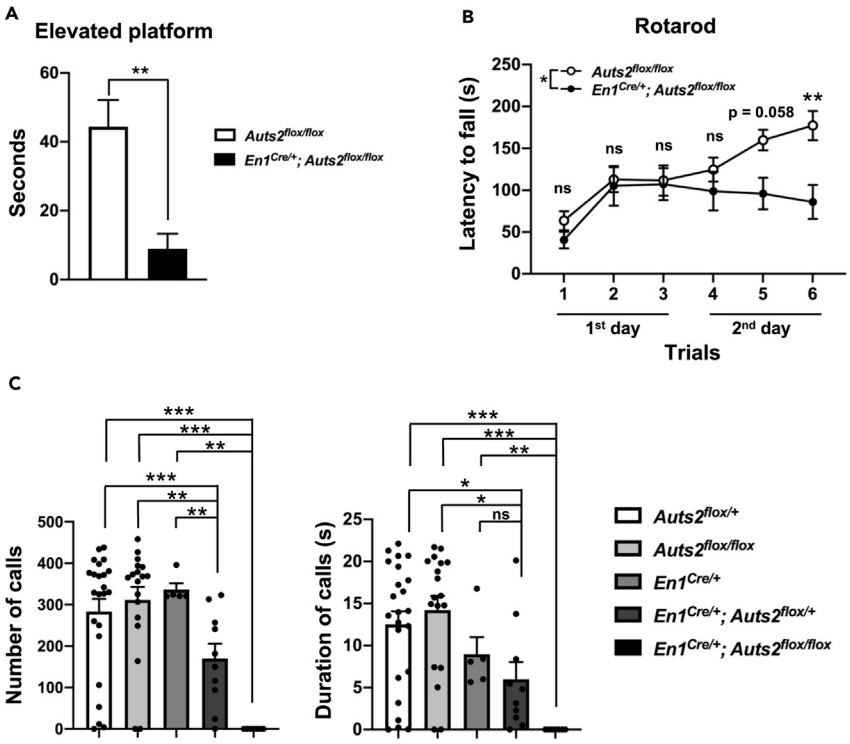

Figure 7. Motor Dysfunction and Impaired Vocal Communication in *Auts2* cKO Mice

(A) *Auts2* cKO mice exhibit motor abnormality in elevated platform test. n = 8 mice.

(B) *Auts2* cKO mice show impaired motor learning in an accelerating rotarod test. n = 13 mice for control mice and 9 mice for *Auts2* cKO mice.

(C) USV recordings show the severe impairments of vocal communication in *Auts2* cKO mice. n = 23 mice for $Auts2^{flox/+}$ mice, 18 mice for $Auts2^{flox/flox}$ mice, 5 mice for $En1^{Cre/+}$ mice, 10 mice for $En1^{Cre/+}$; $Auts2^{flox/+}$ mice, 7 mice for $En1^{Cre/+}$; $Auts2^{flox/flox}$ mice.

Data are shown as mean ± SEM. *p < 0.05, **p < 0.01, ***p < 0.001 by Mann-Whitney test in (A and C), two-way ANOVA followed by Bonferroni's multiple comparisons test in (B).

The Reduced Cerebellar Size in *Auts2* cKO Mice

The *Auts2* cKO mice exhibit a significant reduction in cerebellum size. The volume of the cerebellum is largely determined by the number of GCs that make up the bulk of the cells. Since granule cell precursors (GCPs) proliferate and survive with the support of SHH secreted from PCs (Dahmane and Ruiz i Altaba, 1999), the number of GCs may also be defined by the amount of SHH released from PCs. In the *Auts2* cKO mice, the absolute number of PCs was greatly decreased (Figures 2F and S4), whereas the amount of SHH expressed in the individual PCs did not seem to be altered between *Auts2* cKO mice and the controls (Figure S6). These results imply that the reduction of GCs in *Auts2* cKO mice may be attributed to the diminished number of PCs, resulting in a decrease in the amount of SHH in the cerebellum. During embryonic and postnatal development, we did not find increased apoptosis of PCs (data not shown). Therefore, we believe that PC production from the cerebellar ventricular zone may be reduced in *Auts2* cKO mice, although we do not have any direct evidence. Previous *in situ* hybridization analysis showed that the cerebellar ventricular zone expresses *Auts2* (Bedogni et al., 2010), and, moreover, recent single-cell RNA-sequencing analyses revealed that *Auts2* is expressed in a subpopulation of neural progenitors in both cerebral cortex and cerebellar primordium (Carter et al., 2018; Telley et al., 2019). *In vitro* analyses using mouse embryonic stem cells also demonstrated that the AUTS2-PRC1 complex is critical for neuronal differentiation (Russo et al., 2018). These findings imply that AUTS2 may be involved in production of PCs from the ventricular zone, although that issue is not the focus of this study. As to the decreased size of *Auts2* cKO cerebellum, we cannot rule out the possibility that AUTS2 intrinsically regulates the proliferation of granule cells. Although we did not detect significant levels of AUTS2 protein in the differentiated granule cells with our immunohistochemical conditions, other groups have reported that *Auts2* mRNA is weakly expressed in the neural progenitor cells at the rhombic lip and external granular layer (EGL) of cerebellar

primordium (Bedogni et al., 2010). *Auts2* cKO mice crossed with Cre lines with more restricted expression, such as *Atoh1*-Cre (Fujiyama et al., 2009), will be useful for future studies to explore the role of AUTS2 in cerebellar development.

The Involvement of AUTS2 in PC Maturation

The dendrite morphologies of *Auts2* cKO PCs seemed immature for their developmental ages. The mutant PCs tended to possess multiple primary dendrites on a single soma at P7 and P10 when control PCs usually harbored a single trunk dendrite at those stages. Dendrite height within the ML was also lower for the mutant PCs. These findings suggest *Auts2* cKO PCs are immature for their developmental stages. Because AUTS2 can regulate gene expression as a component of PRC1 (Gao et al., 2014), it is possible that AUTS2 directly or indirectly upregulates genes relevant for PC maturation. Those genes related to PC maturation may regulate PC dendrite development, and their reduced expression may account for the immature dendrite morphology of the *Auts2* cKO PCs. Alternatively, it is also possible that the dendrite morphology of PCs is regulated by cytoplasmic AUTS2. In general, the dendritic morphogenesis is strictly controlled by a variety of cytoskeletal proteins and their regulators. Among them, Rho-family small GTPases such as Cdc42 and Rac1 play pivotal roles in cytoskeletal reorganization during dendrite formation in neurons (Donald et al., 2008; Luo et al., 1996; Puram and Bonni, 2013). We previously reported that the cytoplasmic AUTS2 activates Rac1 via the Rac-GEF, P-Rex1, and Elmo2/Dock180 complexes while downregulating Cdc42 activities via Intersectin 1 and 2. AUTS2-Rac1 signaling is crucial for proper neurite outgrowth and branch formation in cerebral cortical neurons (Hori et al., 2014), implying that AUTS2 may regulate the dendritic morphogenesis of PCs using a common molecular machinery to regulate actin cytoskeleton.

The Involvement of AUTS2 in Synapse Development on PCs

Previous studies indicated that AUTS2 is involved in various neurobiological functions ranging from neuronal proliferation, differentiation as well as neuronal migration and neuritogenesis. Our histological and electrophysiological analyses in this study revealed that AUTS2 is also required for proper synapse formation in PCs. During early postnatal stages, multiple CFs initially innervate a single PC soma, and one single CF is selectively strengthened and begins to form excitatory CF synapses on the PC dendrites, whereas the remaining redundant CF synapses are subsequently eliminated (Kano et al., 2018). PCs also receive an excitatory afferent from PFs of granule cells. PFs compete with CFs to form defined synapse territories on PC dendrites, and PF synaptic activity plays an important role in the pruning of surplus CFs. These CF refinement processes are highly regulated by various synaptic molecules. Among them, *Cacna1a*, a gene encoding P/Q-type voltage-dependent Ca^{2+} channel (also called CaV2.1), plays pivotal role in CF elimination and PF synapse boundary formation during postnatal development (Hashimoto et al., 2011; Miyazaki et al., 2004, 2012). Similar to the synaptic phenotypes in *Auts2* cKO mice, PCs lacking *Cacna1a* exhibit increased PF innervation as well as impaired CF translocation. qPCR and immunohistochemistry revealed that the expression of several synaptic molecules including CaV2.1/*Cacna1a* was decreased in *Auts2* cKO cerebellum. These results raise the possibility that nuclear AUTS2, as a component of PRC1, may participate in CF and PF synapse elimination/formation by regulating the expression of synaptic genes, such as *Cacna1a*. There are few studies reporting the involvement of *Cacna1a* in the dendrite morphogenesis of PCs. Other yet unidentified genes downstream of AUTS2 may also play important roles.

In *Auts2* cKO mice, excessive numbers of dendritic spines were formed in the distal region of PC dendrites. Consistent with this, downregulation of *Auts2* in PCs leads to the enhancement of PF-dependent excitatory neurotransmission. We previously observed that *Auts2* mutant mice exhibited increased spine formation in the forebrain, leading to the enhancement of excitatory synaptic inputs (Hori et al., 2020). A similar phenotype was observed in *Auts2* cKO cerebellum; dendritic spine numbers as well as excitatory inputs were increased without affecting inhibitory inputs in PCs. Because most of the dendritic spines and excitatory inputs we observed should correspond to PF synapses, AUTS2 may also function to restrict the number of PF synapses via its action in the cell nuclei, as was reported for the telencephalon (Hori et al., 2020).

The Involvement of Cerebellar *Auts2* in Motor Function and Social Communication

The cerebellar neural circuit is well-known to be critical for motor coordination as well as motor learning (Apps and Garwicz, 2005). The vestibulocerebellar tract, which projects to lobules IX and X of the nodular cerebellum, carries information for balance (Maklad and Fritzsch, 2003; White and Sillitoe, 2013). We observed that loss of *Auts2* resulted in a reduction in cerebellar size, particularly of cerebellar subregions such as lobe X, Crus I, and copula pyramidis. Consequently, *Auts2* cKO mice displayed impaired motor

control of balance as well as motor learning. These findings raise the possibility that dysgenesis of lobule X observed in *Auts2* cKO cerebellum contributes to the impairment in motor control.

Emerging evidence indicates that activation of PCs by the CF inputs drives motor skill learning such as vestibulo-ocular reflex (VOR) (Nguyen-Vu et al., 2013), whereas disruption of genes involved in synaptic transmission as well as intrinsic calcium signaling in PCs leads to impairment of motor learning (Aiba et al., 1994; Chen et al., 1995; Miyata et al., 2001). AUTS2 potentially regulates the expression of some synapse-related genes such as *Cacna1a*, which may participate in synapse formation required for motor function and learning.

It has previously been reported that loss of GCs or their synaptic functions resulted in behavioral abnormalities, such as motor incoordination and learning defects (Iskusnykh et al., 2018; Sathyanesan et al., 2018; Yoo et al., 2014). It is therefore difficult to distinguish whether the abnormal behaviors observed in this study were caused by the decreased cerebellar size or abnormal synapse formation, although we believe that both morphological alterations might affect behavioral abnormalities.

Recent studies highlighted the important roles for the cerebellum in higher cognitive functions, such as rewarding, social interaction, and social communication in addition to typical motor functions (Carta et al., 2019; Tsai et al., 2012). For example, the transcription factor *FOXP2* (forkhead box P2), is involved in speech in humans, and disruption of *Foxp2* in mice results in cerebellar abnormalities and an absence of vocalization, suggesting an association of the cerebellum with vocal communication (Fujita et al., 2008; Lai et al., 2001; Shu et al., 2005; Usui et al., 2017). Interestingly, Crus I was recently highlighted as a region of the cerebellum linked to cognition, social interaction, and language processing in both rodents and humans (Sokolov et al., 2017; Stoodley et al., 2017). Hence, dysgenesis of Crus I region might be responsible for impairment of vocal communication in *Auts2* cKO mice. Previous clinical studies reported that some individuals with *AUTS2* mutations display microcephaly, motor delay, and speech delay (Amarillo et al., 2014; Sengun et al., 2016). Cerebellar ablation of *Auts2* gene in mice results in a smaller cerebellum and the impairment of vocal communication. Interestingly, impairment of vocal communication was also observed in heterozygous *Auts2* cKO mice. Because most patients carry heterozygous *AUTS2* mutations, we believe heterozygous *Auts2* cKO mice and patients with *AUTS2* mutations may share a common pathology as to communication deficits.

In addition to the cerebellum, the midbrain is also involved in motor control, motivation, and reward behaviors as well as addiction through the dopaminergic neuron system (Hegarty et al., 2013). Emerging studies show that the blockade of the dopamine signaling pathway with dopamine receptor antagonists impairs motor learning (Beeler et al., 2012). Moreover, optogenetic activation of the midbrain dopaminergic neurons induces positive affective USVs in rats (Scardochio et al., 2015), whereas the emission of rat USVs can be repressed by dopamine antagonists (Brudzynski et al., 2012). In mature brains, a large population of dopaminergic neurons reside in the substantia nigra (SN) or ventral tegmental area (VTA) of the ventral midbrain (Hegarty et al., 2013). These dopaminergic neurons arise from the *En1*-derived precursor cells in rhombomere 1 during embryonic stages (Zervas et al., 2004). Bedogni et al. reported that *Auts2* expression is found in TH-positive dopaminergic neurons in the SN and VTA in the midbrain (Bedogni et al., 2010), suggesting that *Auts2* is also disrupted in these neurons in *Auts2* cKO mice. Intriguingly, we found that the TH-positive dopaminergic neurons were reduced in *Auts2* cKO midbrains in adult mice (Figure S5), implying that the potential defects of the dopaminergic pathways in the midbrains may also contribute to the behavioral abnormalities in *Auts2* cKO mice. Interestingly, Oksenberg et al. demonstrated by ChIP-sequencing analysis that AUTS2 binds to the promotor region of a Parkinson disease susceptibility gene, *Uchl1*, in the mouse (Oksenberg et al., 2014). Although further investigations are required to assess how loss of *Auts2* reduces dopaminergic neurons in the midbrain, our findings provide insights into a potential role of AUTS2 in the onset or progression of Parkinson disease or extrapyramidal disorder.

We previously performed behavioral analyses on two types of *Auts2* KO mice. In $Auts2^{neo/+}$ mutants, the expression of all isoforms was reduced approximately by 50%. In the other ($Auts2^{del8/+}$), the expression of FL-AUTS2 and S-AUTS2-Var1 was halved, whereas that of S-AUTS2-Var2 was increased. Interestingly, we observed distinct behavioral abnormalities in social interaction, anxiety, and prepulse inhibition, whereas no difference was detected in USVs. These observations suggested that abnormal overexpression of S-AUTS2-Var2 caused the behavioral abnormalities in those assays, and, therefore, we cannot exclude

the possibility that aberrant expression of S-AUTS2-Var2 may also affect the results of behavioral abnormalities observed in this study.

This is the first investigation, to our knowledge, of the role of AUTS2 in the cerebellar development and function. The pathological mechanisms underlying how defects of cerebellar development caused by loss of AUTS2 function contribute to the psychiatric illnesses remain unclear. Further examination using our *Auts2* cKO mice will help to understand the pathological insights into the neurological disorders caused by *AUTS2* mutations.

Limitations of the Study

Using western blotting, we demonstrated that the expression of FL-AUTS2 and S-AUTS2-Var1 proteins was eliminated in *Auts2* cKO cerebella, whereas that of S-AUTS2-Var2 was increased. Because immunostaining indicated that AUTS2 is expressed only in PCs and Golgi cells, such isoform changes may take place in PCs and Golgi cells in the *Auts2* cKO cerebella. However, it is difficult to confirm such isoform alteration with immunohistochemistry, because currently available AUTS2 antibodies mostly target the C-terminal region that is shared among all isoforms. Future studies to address the expression and function of each AUTS2 isoform in the cerebellum will require the development of better antibodies. With respect to behavioral abnormalities and weight loss, defects in cells other than PCs, namely Golgi and midbrain cells, may be involved. However, an miRNA study that reduced AUTS2 specifically in Purkinje cells resulted in abnormal electrophysiological responses in Purkinje cells, suggesting that impairments of PC maturation and synaptogenesis may likewise be caused by loss of AUTS2 in PCs.

Previously, we demonstrated that the impairments of neurite outgrowth in *Auts2*$^{del8/del8}$ cortical neurons were sufficiently restored by FL-AUTS2 (Hori et al., 2014). Furthermore, aberrant spine formation in the *Auts2*-knockdown (KD) hippocampal neurons were also rescued by FL-AUTS2 but not the AUTS2 short isoforms (Hori et al., 2014). Although we did not assess the effects of loss of S-AUTS2-Var1 for PC dendrite and synapse development, these earlier observations suggest that FL-AUTS2 may regulate dendritic morphogenesis of PCs as well as the development of excitatory synapses on PCs.

The electrophysiological abnormalities in miRNA-introduced PCs were presumably caused by the loss of AUTS2 protein in a cell autonomous manner. However, we cannot exclude the possibility that they may be caused by some non-cell autonomous effects, because miRNA can occasionally be introduced into adjacent PCs.

In the behavioral tests, *Auts2* cKO mice exhibited abnormalities in the elevated platform test and rotarod test, which suggests impairments in motor coordination and learning. However, there remains the possibility that such abnormalities can also be caused by impaired emotional conditions, such as attention deficit or decreased anxiety.

Resource Availability

Lead Contact

Further information and requests for resources should be directed to and will be fulfilled by the Lead Contact, Mikio Hoshino (hoshino@ncnp.go.jp).

Materials Availability

All unique materials generated from this study are available from the Lead Contact with a complete Materials Transfer Agreement.

Data and Code Availability

The datasets or codes in this study are available from the Lead Contact on request.

METHODS

All methods can be found in the accompanying Transparent Methods supplemental file.

SUPPLEMENTAL INFORMATION

Supplemental Information can be found online at https://doi.org/10.1016/j.isci.2020.101820.

ACKNOWLEDGMENTS

This work was supported by Grants-in-Aid for Scientific Research, KAKENHI (Grant 16H06528 and 18H02538 to M.H. and 16K07021 to K.H.) and Grant-in-Aid for JSPS Fellows (Grant 18J10102 to K.Y.); the SRPBS from AMED (19dm0107085h0004), Naito Foundation, Takeda Foundation, Uehara Foundation, Suzuken Memorial Foundation, Princess Takamatsu Cancer Research Fund, an Intramural Research Grant (Grants 30-9 and 1-4 to M.H.). We are grateful to Dr. Ruth Yu (St Jude Children's Research Hospital) for comments on the manuscript.

AUTHORS CONTRIBUTION

K.Y., K.H., E.S.K.L., and M.H. wrote the manuscript and coordinated the project. K.Y., R.A., K.S., N.A., and S.F.E. performed and K.H. supervised imaging experiments and statistical analysis; K.Y., R.A., and A.S. carried out and K.H. supervised behavioral experiments and data analysis; E.S.K.L, T.W., and N.U. performed and M.K. supervised electrophysiological experiments; M.A. and K.S. generated and supervised the designs of *Auts2* mutant mice.

DECLARATION OF INTERESTS

The authors declare no competing interests.

Received: February 3, 2020
Revised: October 19, 2020
Accepted: November 13, 2020
Published: December 18, 2020

REFERENCES

Aiba, A., Kano, M., Chen, C., Stanton, M.E., Fox, G.D., Herrup, K., Zwingman, T.A., and Tonegawa, S. (1994). Deficient cerebellar long-term depression and impaired motor learning in mGluR1 mutant mice. Cell *79*, 377–388.

Altman, J. (1972). Postnatal development of the cerebellar cortex in the rat. II. Phases in the maturation of Purkinje cells and of the molecular layer. J. Comp. Neurol. *145*, 399–463.

Altman, J., and Bayer, S.A. (1978). Prenatal development of the cerebellar system in the rat. II. Cytogenesis and histogenesis of the inferior olive, pontine gray, and the precerebellar reticular nuclei. J. Comp. Neurol. *179*, 49–75.

Alvarez-Saavedra, M., De Repentigny, Y., Lagali, P.S., Raghu Ram, E.V., Yan, K., Hashem, E., Ivanochko, D., Huh, M.S., Yang, D., Mears, A.J., et al. (2014). Snf2h-mediated chromatin organization and histone H1 dynamics govern cerebellar morphogenesis and neural maturation. Nat. Commun. *5*, 4181.

Amaral, D.G., Schumann, C.M., and Nordahl, C.W. (2008). Neuroanatomy of autism. Trends Neurosci. *31*, 137–145.

Amarillo, I.E., Li, W.L., Li, X., Vilain, E., and Kantarci, S. (2014). De novo single exon deletion of AUTS2 in a patient with speech and language disorder: a review of disrupted AUTS2 and further evidence for its role in neurodevelopmental disorders. Am. J. Med. Genet. A *164A*, 958–965.

Apps, R., and Garwicz, M. (2005). Anatomical and physiological foundations of cerebellar information processing. Nat. Rev. Neurosci. *6*, 297–311.

Bauman, M.L., and Kemper, T.L. (2005). Neuroanatomic observations of the brain in autism: a review and future directions. Int. J. Dev. Neurosci. *23*, 183–187.

Bedogni, F., Hodge, R.D., Nelson, B.R., Frederick, E.A., Shiba, N., Daza, R.A., and Hevner, R.F. (2010). Autism susceptibility candidate 2 (Auts2) encodes a nuclear protein expressed in developing brain regions implicated in autism neuropathology. Gene Expr. Patterns *10*, 9–15.

Beeler, J.A., Frank, M.J., McDaid, J., Alexander, E., Turkson, S., Bernardez Sarria, M.S., McGehee, D.S., and Zhuang, X. (2012). A role for dopamine-mediated learning in the pathophysiology and treatment of Parkinson's disease. Cell Rep. *2*, 1747–1761.

Beunders, G., Voorhoeve, E., Golzio, C., Pardo, L.M., Rosenfeld, J.A., Talkowski, M.E., Simonic, I., Lionel, A.C., Vergult, S., Pyatt, R.E., et al. (2013). Exonic deletions in AUTS2 cause a syndromic form of intellectual disability and suggest a critical role for the C terminus. Am. J. Hum. Genet. *92*, 210–220.

Brudzynski, S.M., Komadoski, M., and St Pierre, J. (2012). Quinpirole-induced 50 kHz ultrasonic vocalization in the rat: role of D2 and D3 dopamine receptors. Behav. Brain Res. *226*, 511–518.

Carta, I., Chen, C.H., Schott, A.L., Dorizan, S., and Khodakhah, K. (2019). Cerebellar modulation of the reward circuitry and social behavior. Science *363*, eaav0581.

Carter, R.A., Bihannic, L., Rosencrance, C., Hadley, J.L., Tong, Y., Phoenix, T.N., Natarajan, S., Easton, J., Northcott, P.A., and Gawad, C. (2018). A single-cell transcriptional Atlas of the developing murine cerebellum. Curr. Biol. *28*, 2910–2920 e2912.

Chen, C., Kano, M., Abeliovich, A., Chen, L., Bao, S., Kim, J.J., Hashimoto, K., Thompson, R.F., and Tonegawa, S. (1995). Impaired motor coordination correlates with persistent multiple climbing fiber innervation in PKC gamma mutant mice. Cell *83*, 1233–1242.

Dahmane, N., and Ruiz i Altaba, A. (1999). Sonic hedgehog regulates the growth and patterning of the cerebellum. Development *126*, 3089–3100.

Donald, S., Humby, T., Fyfe, I., Segonds-Pichon, A., Walker, S.A., Andrews, S.R., Coadwell, W.J., Emson, P., Wilkinson, L.S., and Welch, H.C. (2008). P-Rex2 regulates Purkinje cell dendrite morphology and motor coordination. Proc. Natl. Acad. Sci. U S A *105*, 4483–4488.

Elia, J., Gai, X., Xie, H.M., Perin, J.C., Geiger, E., Glessner, J.T., D'Arcy, M., deBerardinis, R., Frackelton, E., Kim, C., et al. (2010). Rare structural variants found in attention-deficit hyperactivity disorder are preferentially associated with neurodevelopmental genes. Mol. Psychiatry *15*, 637–646.

Fujita, E., Tanabe, Y., Shiota, A., Ueda, M., Suwa, K., Momoi, M.Y., and Momoi, T. (2008). Ultrasonic vocalization impairment of Foxp2 (R552H) knockin mice related to speech-language disorder and abnormality of Purkinje cells. Proc. Natl. Acad. Sci. U S A *105*, 3117–3122.

Fujiyama, T., Yamada, M., Terao, M., Terashima, T., Hioki, H., Inoue, Y.U., Inoue, T., Masuyama, N., Obata, K., Yanagawa, Y., et al. (2009). Inhibitory and excitatory subtypes of cochlear nucleus neurons are defined by distinct bHLH transcription factors, Ptf1a and Atoh1. Development *136*, 2049–2058.

Gao, Z., Lee, P., Stafford, J.M., von Schimmelmann, M., Schaefer, A., and Reinberg,

D. (2014). An AUTS2-Polycomb complex activates gene expression in the CNS. Nature *516*, 349–354.

Girirajan, S., Brkanac, Z., Coe, B.P., Baker, C., Vives, L., Vu, T.H., Shafer, N., Bernier, R., Ferrero, G.B., Silengo, M., et al. (2011). Relative burden of large CNVs on a range of neurodevelopmental phenotypes. PLoS Genet. *7*, e1002334.

Hashimoto, K., and Kano, M. (2003). Functional differentiation of multiple climbing fiber inputs during synapse elimination in the developing cerebellum. Neuron *38*, 785–796.

Hashimoto, K., Tsujita, M., Miyazaki, T., Kitamura, K., Yamazaki, M., Shin, H.S., Watanabe, M., Sakimura, K., and Kano, M. (2011). Postsynaptic P/Q-type Ca2+ channel in Purkinje cell mediates synaptic competition and elimination in developing cerebellum. Proc. Natl. Acad. Sci. U S A *108*, 9987–9992.

Hegarty, S.V., Sullivan, A.M., and O'Keeffe, G.W. (2013). Midbrain dopaminergic neurons: a review of the molecular circuitry that regulates their development. Dev. Biol. *379*, 123–138.

Hori, K., and Hoshino, M. (2017). Neuronal migration and AUTS2 syndrome. Brain Sci. *7*, 54.

Hori, K., Nagai, T., Shan, W., Sakamoto, A., Taya, S., Hashimoto, R., Hayashi, T., Abe, M., Yamazaki, M., Nakao, K., et al. (2014). Cytoskeletal regulation by AUTS2 in neuronal migration and neuritogenesis. Cell Rep. *9*, 2166–2179.

Hori, K., Yamashiro, K., Nagai, T., Shan, W., Egusa, S.F., Shimaoka, K., Kuniishi, H., Sekiguchi, M., Go, Y., Tatsumoto, S., et al. (2020). AUTS2 regulation of synapses for proper synaptic inputs and social communication. iScience *23*, 101183.

Iskusnykh, I.Y., Buddington, R.K., and Chizhikov, V.V. (2018). Preterm birth disrupts cerebellar development by affecting granule cell proliferation program and Bergmann glia. Exp. Neurol. *306*, 209–221.

Ito, M. (2006). Cerebellar circuitry as a neuronal machine. Prog. Neurobiol. *78*, 272–303.

Kano, M., Watanabe, T., Uesaka, N., and Watanabe, M. (2018). Multiple phases of climbing fiber synapse elimination in the developing cerebellum. Cerebellum *17*, 722–734.

Kimmel, R.A., Turnbull, D.H., Blanquet, V., Wurst, W., Loomis, C.A., and Joyner, A.L. (2000). Two lineage boundaries coordinate vertebrate apical ectodermal ridge formation. Genes Dev. *14*, 1377–1389.

Kondrychyn, I., Robra, L., and Thirumalai, V. (2017). Transcriptional complexity and distinct expression patterns of auts2 paralogs in Danio rerio. G3 (Bethesda) *7*, 2577–2593.

Lai, C.S., Fisher, S.E., Hurst, J.A., Vargha-Khadem, F., and Monaco, A.P. (2001). A forkhead-domain gene is mutated in a severe speech and language disorder. Nature *413*, 519–523.

Limperopoulos, C., Bassan, H., Gauvreau, K., Robertson, R.L., Jr., Sullivan, N.R., Benson, C.B., Avery, L., Stewart, J., Soul, J.S., Ringer, S.A., et al. (2007). Does cerebellar injury in premature infants contribute to the high prevalence of long-term cognitive, learning, and behavioral disability in survivors? Pediatrics *120*, 584–593.

Luo, L., Hensch, T.K., Ackerman, L., Barbel, S., Jan, L.Y., and Jan, Y.N. (1996). Differential effects of the Rac GTPase on Purkinje cell axons and dendritic trunks and spines. Nature *379*, 837–840.

Maklad, A., and Fritzsch, B. (2003). Development of vestibular afferent projections into the hindbrain and their central targets. Brain Res. Bull. *60*, 497–510.

Mefford, H.C., Muhle, H., Ostertag, P., von Spiczak, S., Buysse, K., Baker, C., Franke, A., Malafosse, A., Genton, P., Thomas, P., et al. (2010). Genome-wide copy number variation in epilepsy: novel susceptibility loci in idiopathic generalized and focal epilepsies. PLoS Genet. *6*, e1000962.

Miyata, M., Kim, H.T., Hashimoto, K., Lee, T.K., Cho, S.Y., Jiang, H., Wu, Y., Jun, K., Wu, D., Kano, M., et al. (2001). Deficient long-term synaptic depression in the rostral cerebellum correlated with impaired motor learning in phospholipase C beta4 mutant mice. Eur. J. Neurosci. *13*, 1945–1954.

Miyazaki, T., Hashimoto, K., Shin, H.S., Kano, M., and Watanabe, M. (2004). P/Q-type Ca2+ channel alpha1A regulates synaptic competition on developing cerebellar Purkinje cells. J. Neurosci. *24*, 1734–1743.

Miyazaki, T., Yamasaki, M., Hashimoto, K., Yamazaki, M., Abe, M., Usui, H., Kano, M., Sakimura, K., and Watanabe, M. (2012). Cav2.1 in cerebellar Purkinje cells regulates competitive excitatory synaptic wiring, cell survival, and cerebellar biochemical compartmentalization. J. Neurosci. *32*, 1311–1328.

Nguyen-Vu, T.D., Kimpo, R.R., Rinaldi, J.M., Kohli, A., Zeng, H., Deisseroth, K., and Raymond, J.L. (2013). Cerebellar Purkinje cell activity drives motor learning. Nat. Neurosci. *16*, 1734–1736.

Oksenberg, N., and Ahituv, N. (2013). The role of AUTS2 in neurodevelopment and human evolution. Trends Genet. *29*, 600–608.

Oksenberg, N., Haliburton, G.D., Eckalbar, W.L., Oren, I., Nishizaki, S., Murphy, K., Pollard, K.S., Birnbaum, R.Y., and Ahituv, N. (2014). Genome-wide distribution of Auts2 binding localizes with active neurodevelopmental genes. Transl. Psychiatry *4*, e431.

Oksenberg, N., Stevison, L., Wall, J.D., and Ahituv, N. (2013). Function and regulation of AUTS2, a gene implicated in autism and human evolution. PLoS Genet. *9*, e1003221.

Patrizi, A., Scelfo, B., Viltono, L., Briatore, F., Fukaya, M., Watanabe, M., Strata, P., Varoqueaux, F., Brose, N., Fritschy, J.M., et al. (2008). Synapse formation and clustering of neuroligin-2 in the absence of GABAA receptors. Proc. Natl. Acad. Sci. U S A *105*, 13151–13156.

Puram, S.V., and Bonni, A. (2013). Cell-intrinsic drivers of dendrite morphogenesis. Development *140*, 4657–4671.

Russo, D., Della Ragione, F., Rizzo, R., Sugiyama, E., Scalabri, F., Hori, K., Capasso, S., Sticco, L., Fioriniello, S., De Gregorio, R., et al. (2018). Glycosphingolipid metabolic reprogramming drives neural differentiation. EMBO J. *37*, e97674.

Sathyanesan, A., Kundu, S., Abbah, J., and Gallo, V. (2018). Neonatal brain injury causes cerebellar learning deficits and Purkinje cell dysfunction. Nat. Commun. *9*, 3235.

Scardochio, T., Trujillo-Pisanty, I., Conover, K., Shizgal, P., and Clarke, P.B. (2015). The effects of electrical and optical stimulation of midbrain dopaminergic neurons on rat 50-kHz ultrasonic vocalizations. Front. Behav. Neurosci. *9*, 331.

Schmahmann, J.D., and Caplan, D. (2006). Cognition, emotion and the cerebellum. Brain *129*, 290–292.

Schmahmann, J.D., and Sherman, J.C. (1998). The cerebellar cognitive affective syndrome. Brain *121* (Pt 4), 561–579.

Sengun, E., Yararbas, K., Kasakyan, S., and Alanay, Y. (2016). AUTS2 Syndrome in a 68-year-old female: natural history and further delineation of the phenotype. Am. J. Med. Genet. A *170*, 3231–3236.

Sgaier, S.K., Lao, Z., Villanueva, M.P., Berenshteyn, F., Stephen, D., Turnbull, R.K., and Joyner, A.L. (2007). Genetic subdivision of the tectum and cerebellum into functionally related regions based on differential sensitivity to engrailed proteins. Development *134*, 2325–2335.

Shu, W., Cho, J.Y., Jiang, Y., Zhang, M., Weisz, D., Elder, G.A., Schmeidler, J., De Gasperi, R., Sosa, M.A., Rabidou, D., et al. (2005). Altered ultrasonic vocalization in mice with a disruption in the Foxp2 gene. Proc. Natl. Acad. Sci. U S A *102*, 9643–9648.

Sillitoe, R.V., and Joyner, A.L. (2007). Morphology, molecular codes, and circuitry produce the three-dimensional complexity of the cerebellum. Annu. Rev. Cell Dev. Biol. *23*, 549–577.

Singec, I., Knoth, R., Ditter, M., Frotscher, M., and Volk, B. (2003). Neurogranin expression by cerebellar neurons in rodents and non-human primates. J. Comp. Neurol. *459*, 278–289.

Sokolov, A.A., Miall, R.C., and Ivry, R.B. (2017). The cerebellum: adaptive prediction for movement and cognition. Trends Cogn. Sci. *21*, 313–332.

Sotelo, C., and Dusart, I. (2009). Intrinsic versus extrinsic determinants during the development of Purkinje cell dendrites. Neuroscience *162*, 589–600.

Stoodley, C.J., D'Mello, A.M., Ellegood, J., Jakkamsetti, V., Liu, P., Nebel, M.B., Gibson, J.M., Kelly, E., Meng, F., Cano, C.A., et al. (2017). Altered cerebellar connectivity in autism and cerebellar-mediated rescue of autism-related behaviors in mice. Nat. Neurosci. *20*, 1744–1751.

Takeo, Y.H., Kakegawa, W., Miura, E., and Yuzaki, M. (2015). RORalpha regulates multiple aspects of dendrite development in cerebellar Purkinje cells in vivo. J. Neurosci. *35*, 12518–12534.

Talkowski, M.E., Rosenfeld, J.A., Blumenthal, I., Pillalamarri, V., Chiang, C., Heilbut, A., Ernst, C., Hanscom, C., Rossin, E., Lindgren, A.M., et al. (2012). Sequencing chromosomal abnormalities

reveals neurodevelopmental loci that confer risk across diagnostic boundaries. Cell *149*, 525–537.

Telley, L., Agirman, G., Prados, J., Amberg, N., Fievre, S., Oberst, P., Bartolini, G., Vitali, I., Cadilhac, C., Hippenmeyer, S., et al. (2019). Temporal patterning of apical progenitors and their daughter neurons in the developing neocortex. Science *364*, eaav2522.

Tsai, P.T., Hull, C., Chu, Y., Greene-Colozzi, E., Sadowski, A.R., Leech, J.M., Steinberg, J., Crawley, J.N., Regehr, W.G., and Sahin, M. (2012). Autistic-like behaviour and cerebellar dysfunction in Purkinje cell Tsc1 mutant mice. Nature *488*, 647–651.

Usui, N., Co, M., Harper, M., Rieger, M.A., Dougherty, J.D., and Konopka, G. (2017). Sumoylation of FOXP2 regulates motor function and vocal communication through Purkinje cell development. Biol. Psychiatry *81*, 220–230.

Van Overwalle, F., Baetens, K., Marien, P., and Vandekerckhove, M. (2014). Social cognition and the cerebellum: a meta-analysis of over 350 fMRI studies. Neuroimage *86*, 554–572.

White, J.J., and Sillitoe, R.V. (2013). Development of the cerebellum: from gene expression patterns to circuit maps. Wiley Interdiscip. Rev. Dev. Biol. *2*, 149–164.

Yamasaki, M., Miyazaki, T., Azechi, H., Abe, M., Natsume, R., Hagiwara, T., Aiba, A., Mishina, M., Sakimura, K., and Watanabe, M. (2011). Glutamate receptor delta2 is essential for input pathway-dependent regulation of synaptic AMPAR contents in cerebellar Purkinje cells. J. Neurosci. *31*, 3362–3374.

Yoo, J.Y., Mak, G.K., and Goldowitz, D. (2014). The effect of hemorrhage on the development of the postnatal mouse cerebellum. Exp. Neurol. *252*, 85–94.

Yuasa, S., Kawamura, K., Ono, K., Yamakuni, T., and Takahashi, Y. (1991). Development and migration of Purkinje cells in the mouse cerebellar primordium. Anat. Embryol. (Berl) *184*, 195–212.

Zervas, M., Millet, S., Ahn, S., and Joyner, A.L. (2004). Cell behaviors and genetic lineages of the mesencephalon and rhombomere 1. Neuron *43*, 345–357.

iScience, Volume *23*

Supplemental Information

AUTS2 Governs Cerebellar Development, Purkinje Cell Maturation, Motor Function and Social Communication

Kunihiko Yamashiro, Kei Hori, Esther S.K. Lai, Ryo Aoki, Kazumi Shimaoka, Nariko Arimura, Saki F. Egusa, Asami Sakamoto, Manabu Abe, Kenji Sakimura, Takaki Watanabe, Naofumi Uesaka, Masanobu Kano, and Mikio Hoshino

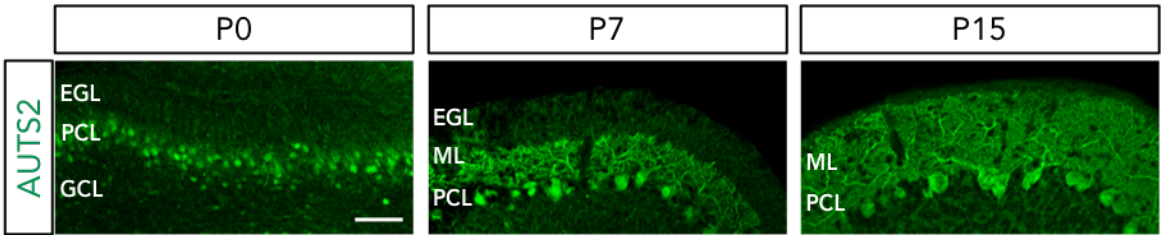

Figure S1. AUTS2 expression in PCs during postnatal cerebellar development, Related to Figure 1.

Representative images of the PCs stained with anti-AUTS2 antibody in WT developing cerebellum at P0, 7 and 15. Scale bar, 50 μm.

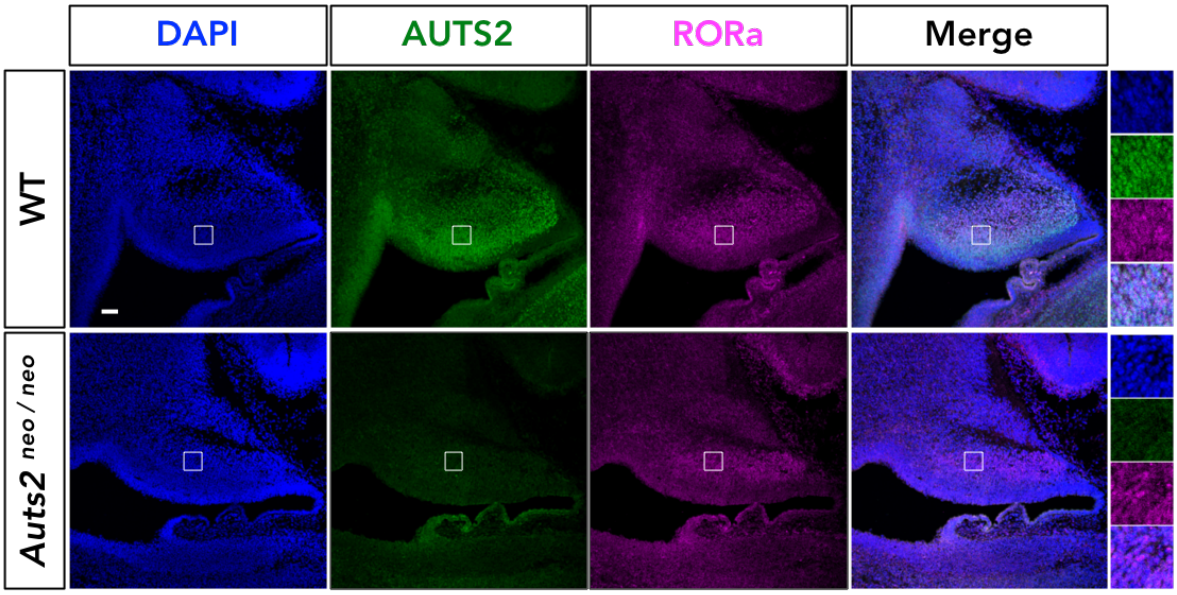

Figure S2. Characterization of the specificity of anti-AUTS2 antibody, Related to Figure 2.

Immunostaining on the sagittal sections of the developing cerebellum (E13.5) using the AUTS2 antibody showing the disappearance of AUTS2 immuno-signals in the RORa-positive PCs of *Auts2*$^{neo/neo}$ homozygotic mutants. Scale bar, 50 μm.

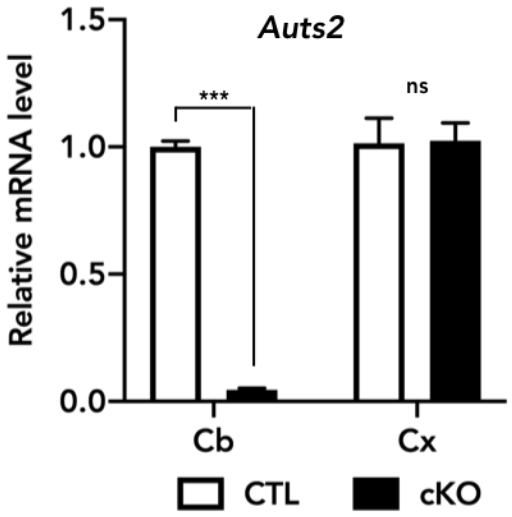

Figure S3. Conditional deletion of *Auts2* gene in *Auts2* cKO cerebellum, Related to Figure 2.

Auts2 mRNA levels in the cerebellum (Cb) and cerebral cortex (Cx) of neonatal *Auts2* cKO homozygotic mutant mice and control mice (CTL). qPCR was performed using primers specific for the deleted exon (n=3-4 mice). Data are shown as mean ± SEM. ***p<0.001, unpaired t-test with Welch's correction.

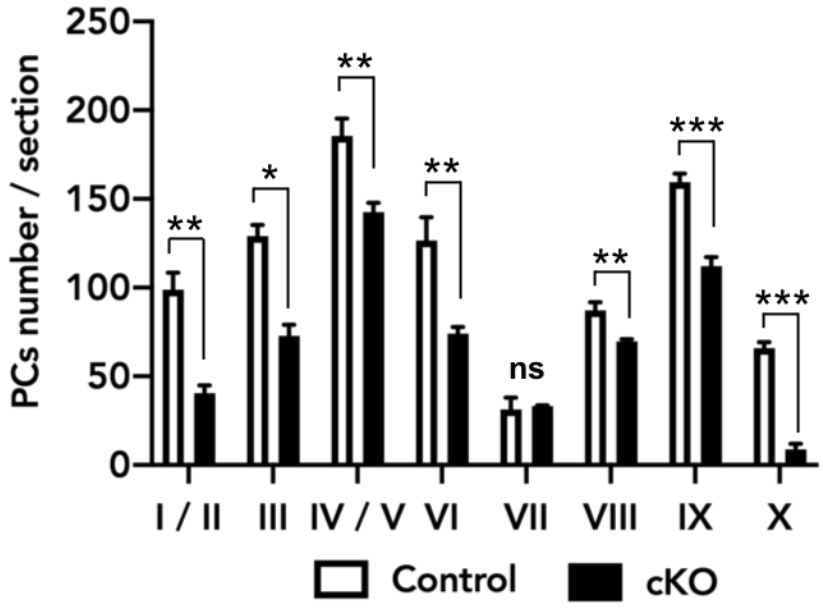

Figure S4. Loss of *Auts2* results in the reduction of PCs, Related to Figure 2.

Graph showing the measurements of the number of PCs at each lobule in sagittal cerebellar vermis sections from adult *Auts2* cKO mutants and control mice (n=4 mice). Data are shown as mean ± SEM. ***p<0.001, Mann-Whitney U test.

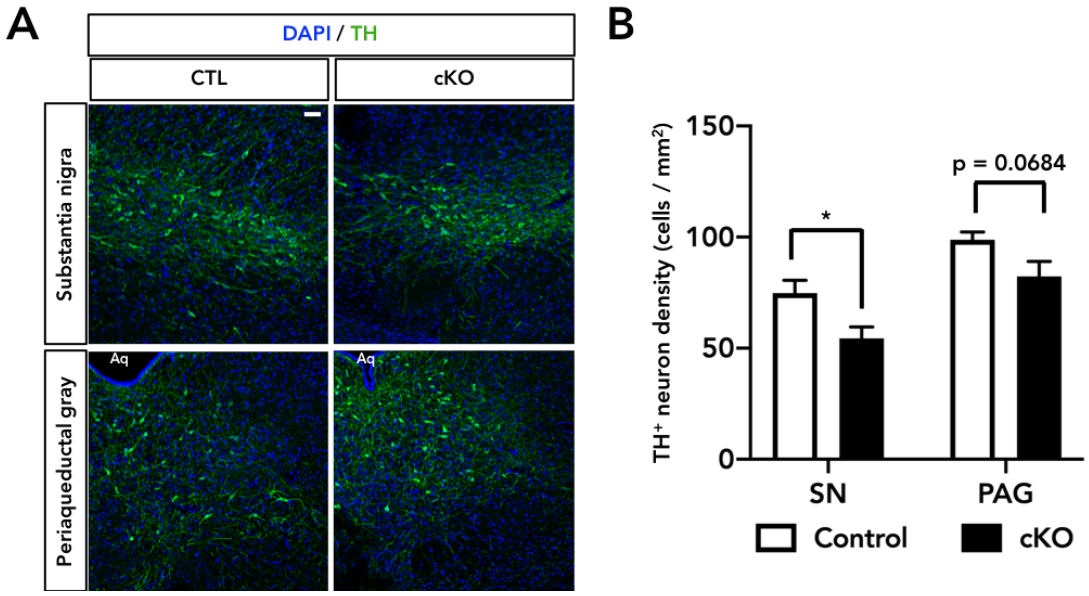

Figure S5. Characterization of the dopaminergic neurons in *Auts2* cKO midbrains, Related to Figure 2.

(A) Immunofluorescence on coronal midbrain sections from P20 control and *Auts2* cKO mice using anti-tyrosine hydroxylase (TH) antibody. Aq: aqueduct of midbrain. (B) Graph shows the density of the TH-positive dopaminergic neurons at substantia nigra (SN) and periaqueductal gray (PAG) in *Auts2* cKO mice and controls (n=4-12 areas, 3 mice). Dopaminergic neurons were reduced in the SN of *Auts2* cKO mutants. Data are presented as mean ± SEM. P<0.05, unpaired t-test. Scale bar, 50 μm.

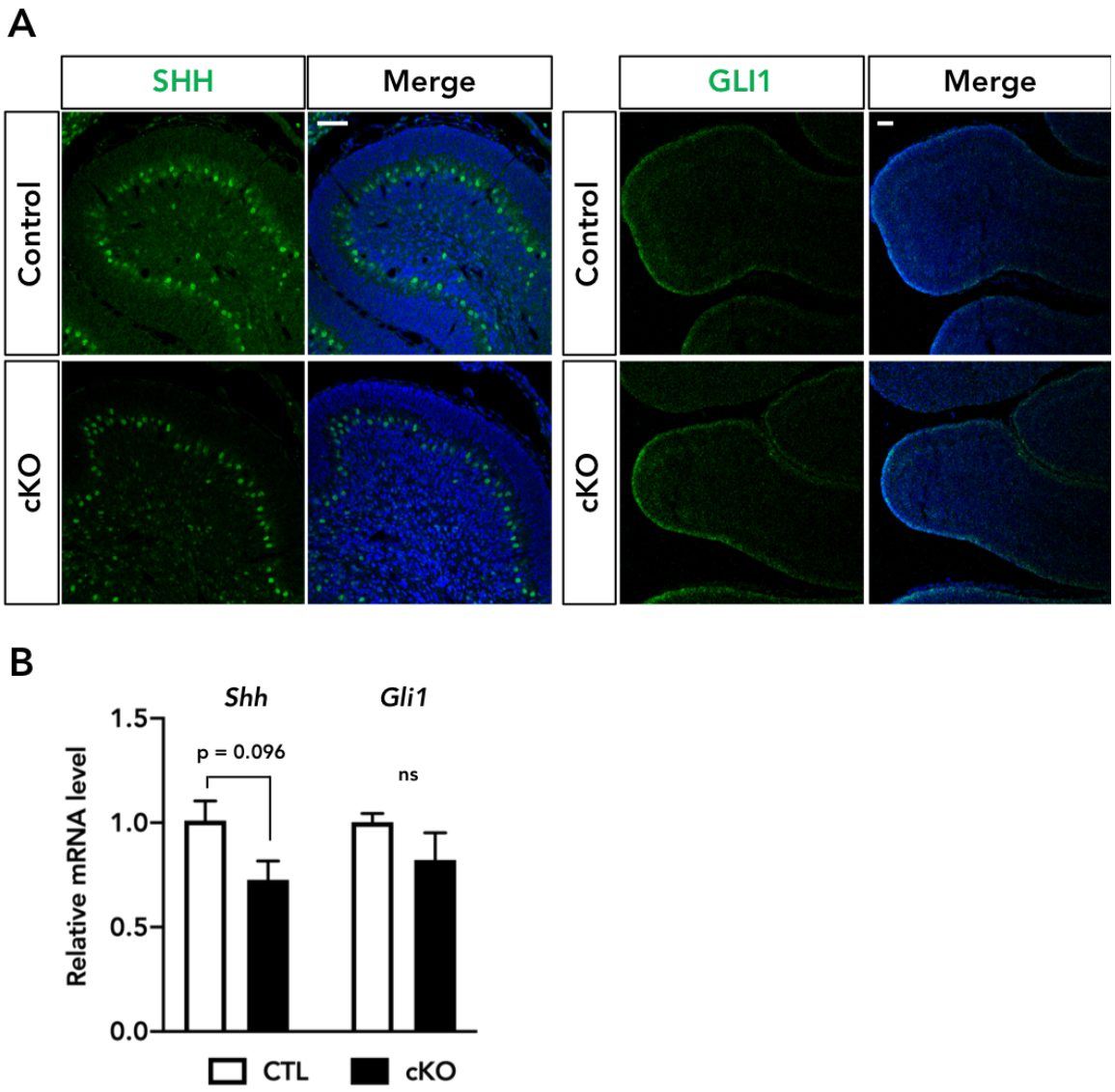

Figure S6. Normal SHH signaling in the developing cerebellum of *Auts2* cKO mice, Related to Figure 2.

(A) Representative images of the postnatal (P7) sagittal cerebellar tissue sections from *Auts2* cKO mutant and control mice stained with SHH (left panels) and GLI1 (right panels). (B) Graph shows the measurements of the transcript levels of SHH-signaling molecules in *Auts2* cKO and control mice (n=3 mice) at P7. Data are shown as mean ± SEM. ns, not significant, unpaired t-test with Welch's correction.

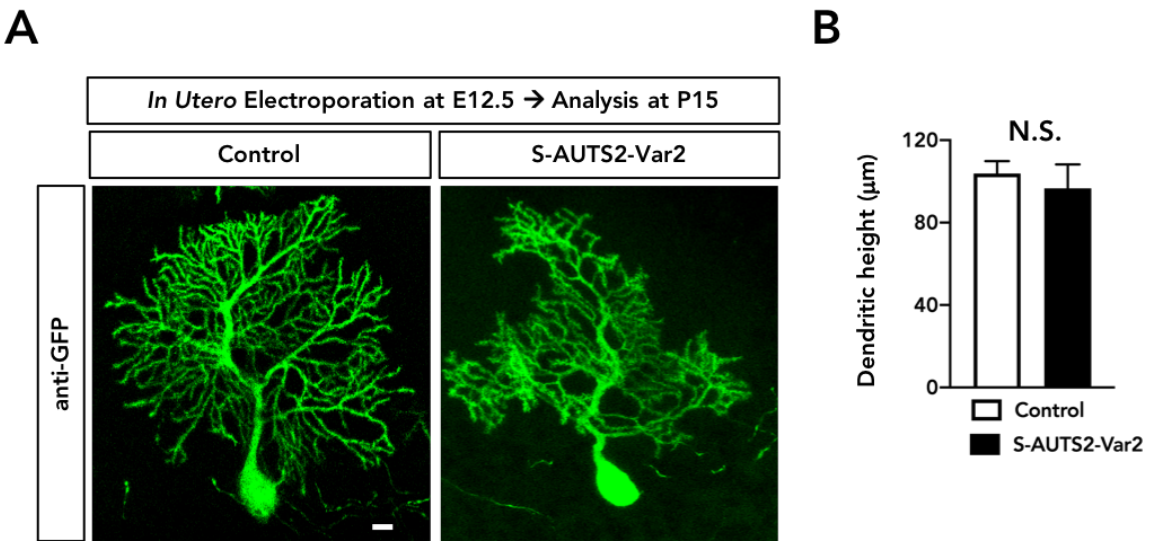

Figure S7. Overexpression of S-AUTS2-Var2 does not affect dendritic outgrowth of PCs, Related to Figure 3.

(A) Representative images of control (EGFP) and S-AUTS2-Var2-overexpressed PCs at P15. The expression vectors were electroporated into WT embryonic cerebellum at E12.5 and tissues were analyzed at P15. (B) Measurement of dendrite lengths of PCs toward the pial surface. n=6-8 cells from N=2-3 mice. N.S., not significant, Mann-Whitney U test. Scale bar, 20 μm.

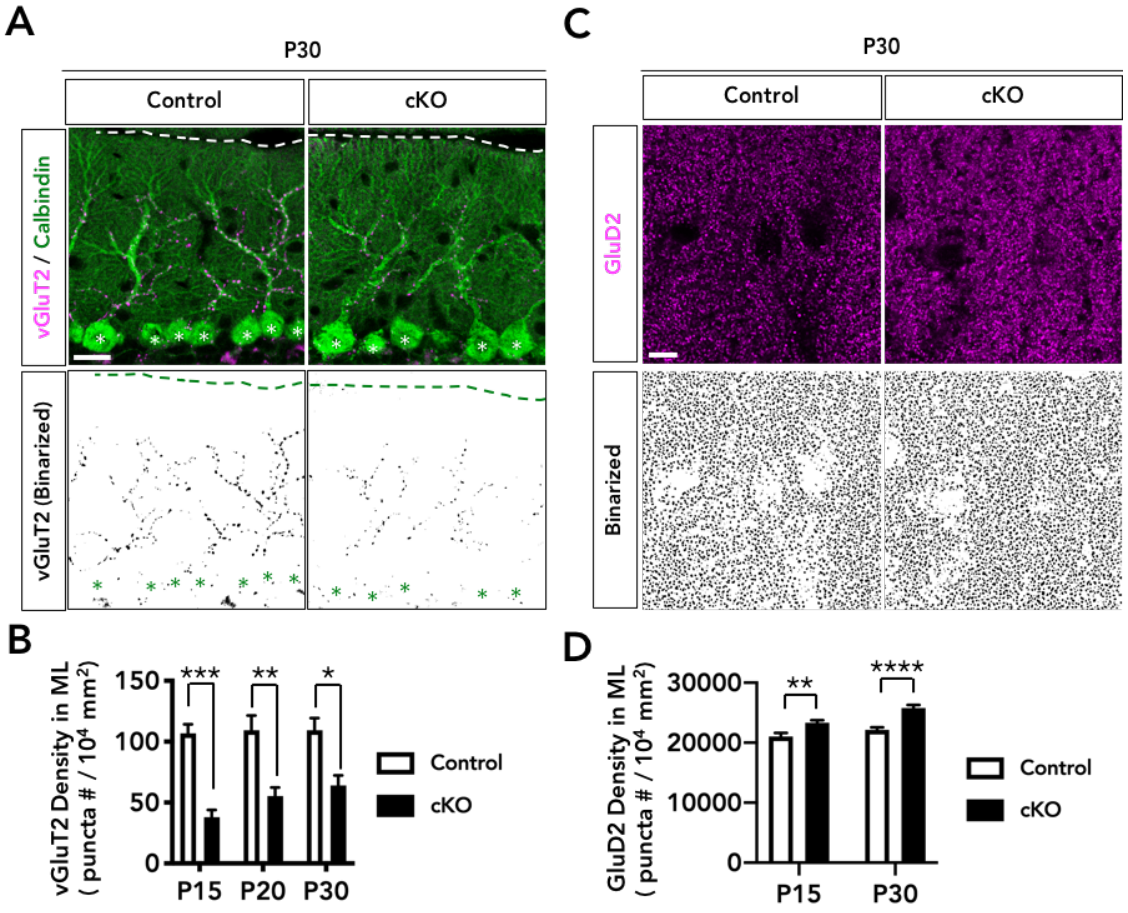

Figure S8. The density of CF and PF synapses in *Auts2* cKO mice during postnatal development, Related to Figure 4.

(A) Representative images showing double immunostaining with Calbindin (green) and vGluT2 (magenta) in P30 control and *Auts2* cKO mice in lobule IV/V. The vGluT2 immunoreactivities are binarized in the bottom. Dotted lines and asterisks indicate pial surface of the ML and PC soma, respectively. (B) Quantification of the density of vGluT2 puncta in ML from P15 to P30 control and *Auts2* cKO cerebellum (n = 4-6 areas from N = 2-3 mice). (C) Representative images showing immunostaining with GluD2 (magenta) in P30 control and *Auts2* cKO mice in the ML with high magnification. The GluD2-immunoreactivities are binarized at the bottom. (D) Measurements of the GluD2 puncta density in ML of control and *Auts2* cKO mice at P15 and P30 (n = 40-54 areas from 3 mice). Data are shown as mean ± SEM. *p < 0.05, **p < 0.01, ***p < 0.001, ****p < 0.0001 by unpaired t-test with Welch's correction in (B) and Mann-Whitney U test in (D). Scale bar, 20 μm in (A) and 5 μm in (C).

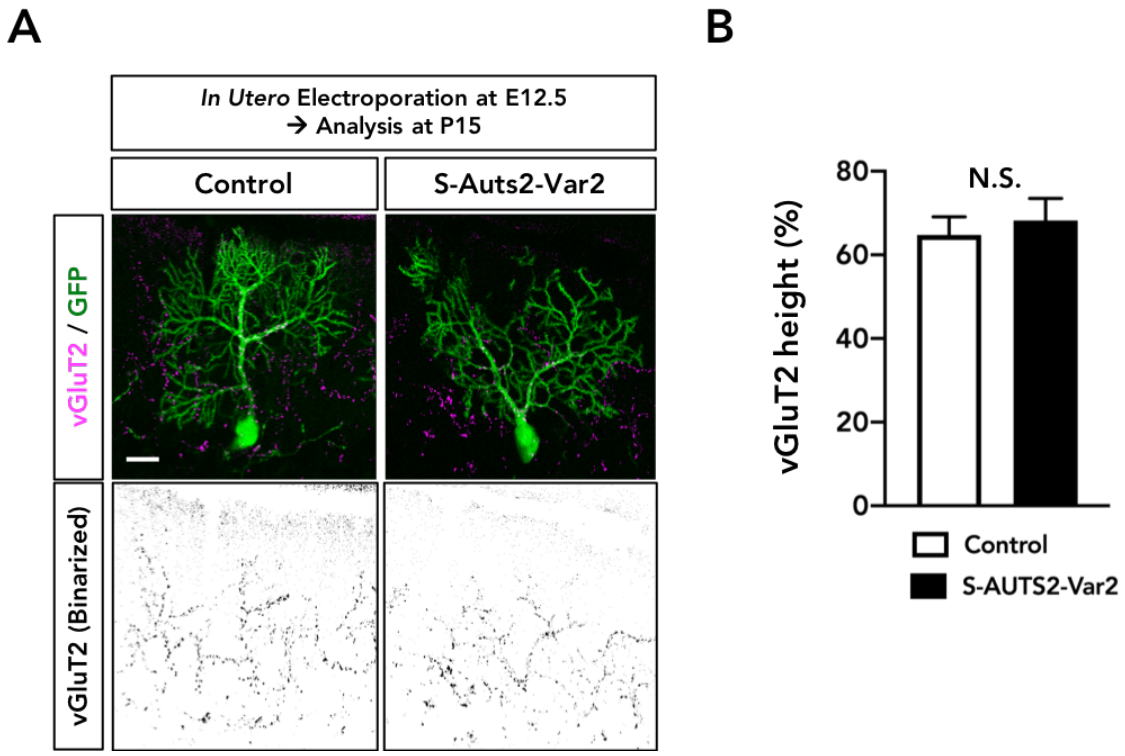

Figure S9. S-AUTS2-Var2-overexpressed PCs exhibit normal CF translocation, Related to Figure 4.

(A) Representative images of EGFP (control) and S-AUTS2-Var2-overexpressed PCs at P15. The expression vectors were introduced by *in utero* electroporation into WT embryonic cerebellum at E12.5 and cerebellar tissues stained with anti-GFP (green) and vGluT2 (magenta) were analyzed at P15. The vGluT2-immunoreactivities are binarized at the bottom. (B) Quantitative analysis of the ratio of vGluT2 height to the tip of PC dendrites (n =6 cells from 3 mice). Data are shown as mean ± SEM. N.S., not significant, unpaired t-test. Scale bar, 20 μm.

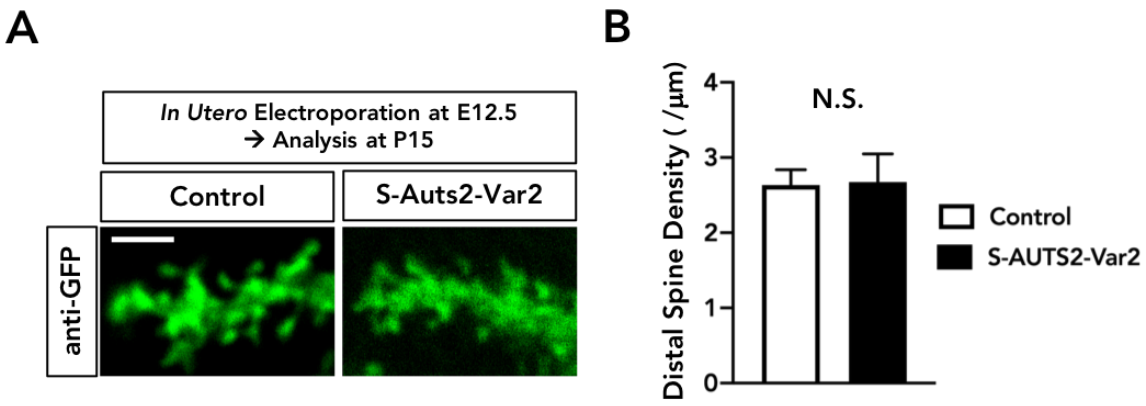

Figure S10. Characterization of dendritic spine formation in S-AUTS2-Var2-overexpressed PCs, Related to Figure 4.

(A) Representative images of the spines on the distal end of dendrites from control (EGFP) and S-AUTS2-Var2-overexpressed PCs at P15. Expression plasmids were electroporated into WT embryonic cerebellum at E12.5. (B) Quantification of the dendritic spine density on the distal end of dendrites from control and S-AUTS2-Var2-overexpressed PCs at P15 (n=5-6 dendrites from 2-3 mice). Data are presented as mean ± SEM. N.S., not significant, Mann-Whitney U test. Scale bar, 2 μm.

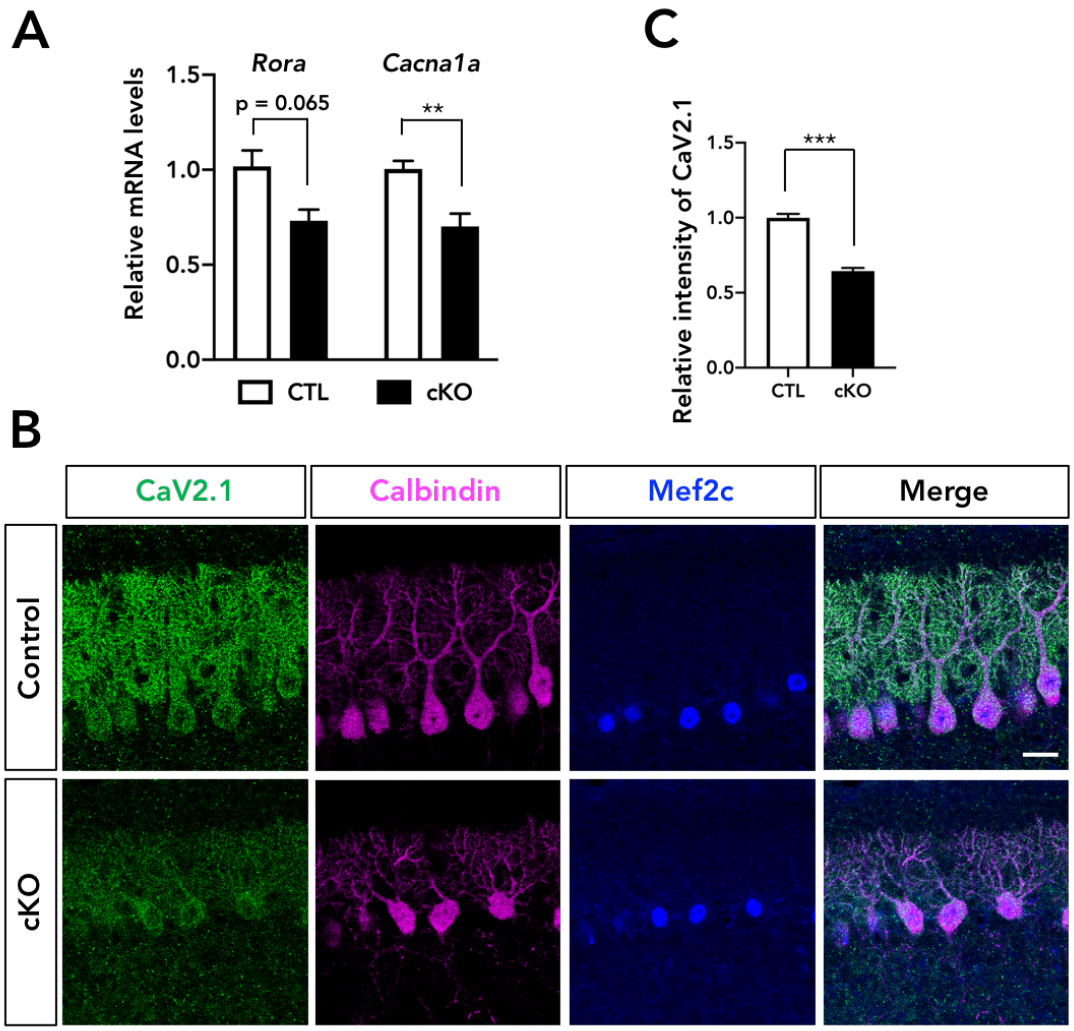

Figure S11. Downregulation of CaV2.1 in the PCs of *Auts2* cKO mice, Related to Figure 4.

(A) qRT-PCR results show that expression levels of *Cacna1a*, but not *Rora*, was significantly reduced in *Auts2* cKO mice at P7 (n = 6 mice). (B) Representative images of triple-immunostaining with CaV2.1(green), Calbindin (magenta) and Mef2c (blue) in P10 control and *Auts2* cKO mice in cerebellar lobule VI. (C) Decreased immunofluorescence intensity levels of CaV2.1 normalized with Mef2c in PCs in control and *Auts2* cKO mice. n=357-375 cells, 3 mice. Data are shown as mean ± SEM. **p < 0.01, ***p < 0.001 by unpaired t-test (A) and Mann-Whitney test (B). Scale bar, 20 μm.

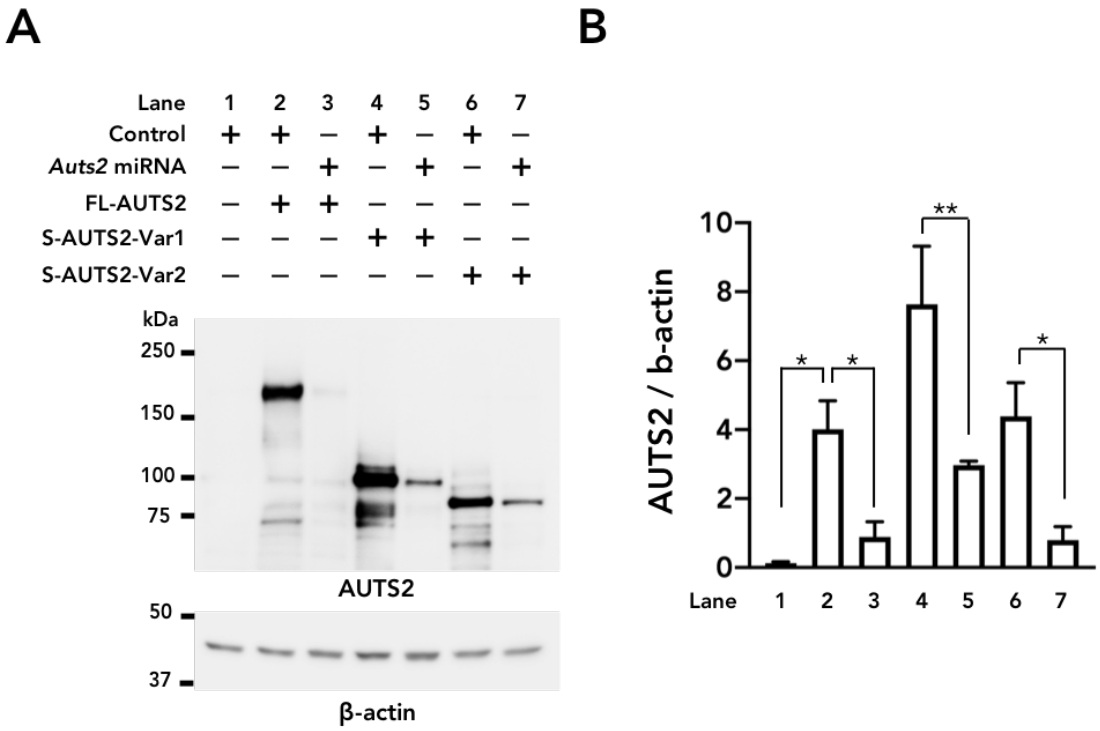

Figure S12. The efficacy of *Auts2* miRNA vector, Related to Figures 5 and 6.

(A) Representative images showing lysates of HEK293T cells transfected with or without control (pCL20c-trL7), *Auts2* miRNA, FL-AUTS2, S-AUTS2-Var1 and S-AUTS2-Var2 expression vector that were immunoblotted with AUTS2 and β-actin antibodies. (B) Quantification of AUTS2 protein levels normalized with β-actin. N = 3 cells for lane 1 (control only), 2 (control and FL-AUTS2), 3 (*Auts2* miRNA and FL-AUTS2), 6 (control and S-AUTS2-Var2) and 7 (*Auts2* miRNA and S-AUTS2-Var2); N = 5 cells for lane 4 (control and S-AUTS2-Var1) and 5 (*Auts2* miRNA and S-AUTS2-Var1). Data are shown as mean ± SEM. *$p < 0.05$, **$p < 0.01$, by Mann-Whitney U test or unpaired t-test with Welch's correction in (B).

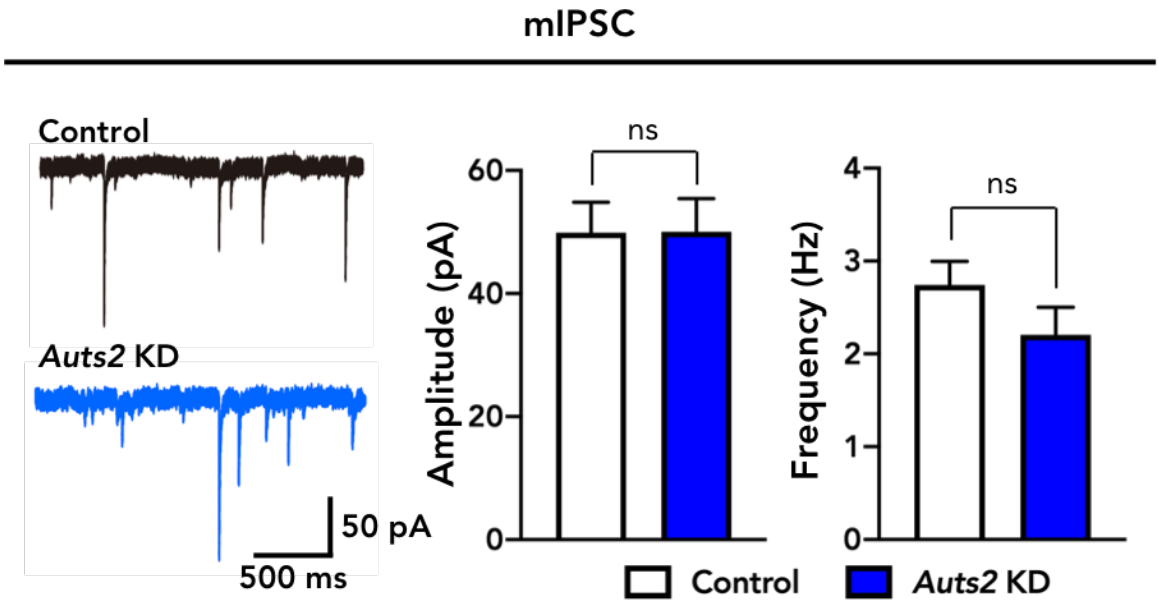

Figure S13. Normal mIPSC in *Auts2*-KD PCs, Related to Figures 5.

No effect of mIPSC in *Auts2*-KD PCs at P20-30. Panels depict representative mIPSC traces (left) and summary graphs of the mIPSC amplitude and frequency in control and *Auts2*-KD PCs. n= 19 cells, 6 mice for control and n= 18 cells, 6 mice for *Auts2* KD. Data are shown as mean ± SEM. ns; not significant, unpaired student t-test.

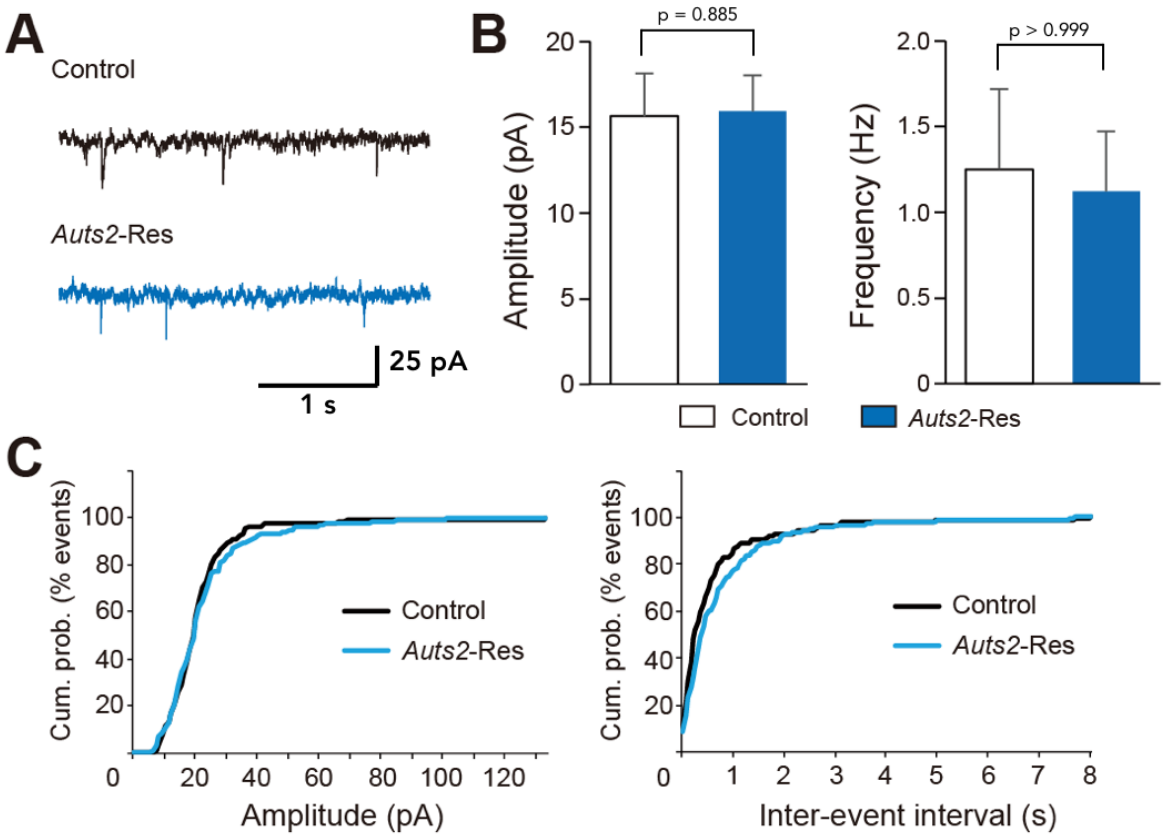

Figure S14. Co-transfection of an RNAi-resistant *Auts2* with the *Auts2* targeted miRNA normalizes enhanced excitatory synaptic transmission by *Auts2* knockdown, Related to Figures 5.

(A) Sample traces of mEPSCs for non-transfected (control) and transfected (*Auts2* KD + *Auts2*-Res) PCs. (B) Summary bar graphs showing the amplitude and frequency of mEPSCs for control (white columns, n = 9 cells from 4 mice) and *Auts2* KD + *Auts2*-Res (blue columns, n = 9 cells from 4 mice) PCs at P20-30. (C) Cumulative probability distributions of mEPSC amplitudes (left) and inter-event intervals (right) in control and *Auts2*-Res PCs. No significant differences were found. Data are shown as mean ± SEM. Mann-Whitney test in (B).

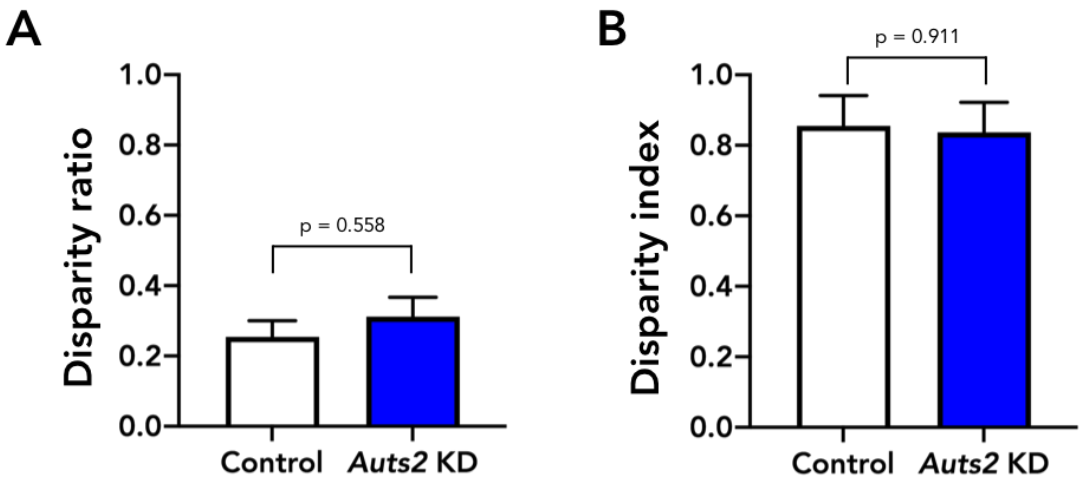

Figure S15. Knockdown of *Auts2* in PCs does not affect the selective strengthening of single CFs at P20-30, Related to Figures 6.

(A, B) Quantification of the disparity ratio (A) showing the relative differences among the strengths of multiple CF-EPSCs, and of the disparity index (B) indicating the coefficient of variation for all CF-EPSC amplitudes measured in a given PC. Methods for calculation are as previously described. n= 6 cells, 3 mice for control and n= 20 cells, 4 mice for *Auts2* KD. Data are shown as mean ± SEM. Unpaired student t-test in (A) and (B).

	Control	*Auts2* KD	P value
Amplitudes (nA)	2.30 ± 0.14	2.93 ± 0.27	0.059
10%-90% Rise Time (ms)	0.47 ± 0.02	0.57 ± 0.03	0.007**
Decay Time constant (ms)	5.26 ± 0.24	4.27 ± 0.24	0.006**
N(cells, mice)	(23, 3)	(26, 4)	

Table S1. Summary of electrophysiological characterization of the strongest CF-EPSCs in control and *Auts2* knockdown PCs at P20-30, Related to Figures 6.

Data are shown as mean ± SEM. p** < 0.01, unpaired Student's t-test.

Transparent Methods

Experimental animals

All animal experiments were conducted in accordance with the guidelines for the Animal Care and Use Committee of the National Center of Neurology and Psychiatry, and for the care and use of laboratory animals of the University of Tokyo and the Japan Neuroscience Society. *Engrailed-1*$^{Cre/+}$ (*En1*$^{Cre/+}$) mice and *Auts2-floxed* mice have been described previously (Hori et al., 2014; Kimmel et al., 2000). *En1*$^{Cre/+}$ mice were obtained from The Jackson Laboratory. *En1*$^{Cre/+}$ mice and *Auts2-floxed* mice were maintained in the C57BL/6N background. *En1*$^{Cre/+}$ *;Auts2*$^{flox/flox}$ homozygous mice were generated by crossing *En1*$^{Cre/+}$ mice with *Auts2*$^{flox/flox}$ mice to obtain *En1*$^{Cre/+}$ *;Auts2*$^{flox/+}$ heterozygous mutant progeny. *En1*$^{Cre/+}$ *;Auts2*$^{flox/+}$ male mice were crossed with *Auts2*$^{flox/flox}$ female mice to yield litters of control mice (*Auts2*$^{flox/+}$ or *Auts2*$^{flox/flox}$), heterozygous (*En1*$^{Cre/+}$ *;Auts2*$^{flox/+}$) and homozygous (*En1*$^{Cre/+}$ *;Auts2*$^{flox/flox}$) mutant mice. Unless otherwise indicated, *Auts2*$^{flox/flox}$ mice were used as the control in this study. Mice were maintained in ventilated racks under a 12-h light/dark cycle. Food and water were provided *ad libitum* in temperature controlled, pathogen-free facilities. Only littermate male mice were used for behavioral tests.

Plasmids

The plasmid construction of pCAG-Myc-AUTS2-full length, pCAG-Myc-AUTS2-var1, pCAG-Myc-AUTS2-var2 were previously described (Hori et al., 2014). For *Auts2* knockdown, the plasmid DNAs were designed to express EGFP and/or microRNA (miRNA) directed against *Auts2* under the control of a truncated L7 promoter (pCL20c-trL7) (Sawada et al., 2010). Engineered microRNAs (5'-TGCTGATAAAGTGGAAGGTCGTGCCAGTTTTGGCCACTGACTGACTGGCACGATTCCACTTTAT-3' and 5'-CCTGATAAAGTGGAATCGTGCCAGTCAGTCAGTGGCCAAAACTGGCACGACCTTCCACTTTATC-3') were designed against the mouse *Auts2* coding sequence using the BLOCK-iT Pol II miR RNAi Expression Vector Kit guidelines (Invitrogen). *Auts2* miRNA constructs were subcloned into the pCL20c-trL7. For *Auts2* rescue experiments, the cDNA for *Auts2* was obtained by PCR of a cDNA library from the cerebellum of P10 mice. The QuikChange Lightning site-directed mutagenesis kit (#210518, Agilent Technologies) was used to generate RNAi-resistant forms of *Auts2* (*Auts2*-Res) in which seven nucleotides were mutated without changing the amino acid sequence in the miRNA targeted site. *Auts2*-Res was linked in-frame to EGFP interposed by a picornavirus "self-cleaving" P2A peptide sequence to enable efficient bicistronic expression. The cDNA was subcloned into pCL20c-trL7.

Immunostaining and Nissl staining

Whole brains were dissected out after mice were transcardially perfused with 4% paraformaldehyde (PFA) or periodate-lysine-paraformaldehyde (PLP) in 0.1M sodium phosphate buffer (pH 7.2) under deep isoflurane anesthesia. The brains were further fixed in 4% PFA or PLP for 2 hrs to overnight, cryoprotected with 30% sucrose, embedded in O.C.T. compound (Sakura Fine-Tek, Tokyo, Japan), and cryosectioned at 20 μm. Parasagittal sections were treated with blocking solution containing 1% normal donkey serum (Merck Millipore, Burlington, MA, USA) and 0.2% TX-100 (Nacalai Tesque, Kyoto, Japan) for 1 h at room temperature and immunolabeled using the following primary antibodies in blocking solution at 4 °C overnight: goat-AUTS2 (1:300, EB09003, Everest Biotech, Bicester, UK), rabbit-AUTS2 (1:500, HPA000390, Sigma-Aldrich, St. Louis, MO, USA), rabbit-cleaved Caspase 3 (1:500, 9661S, Cell Signaling Technology, Danvers, MA, USA), rabbit-Calbindin (1:500, AB1778, Merck Millipore), goat-Calbindin (1:1000, Calbindin-Go-Af1040, Frontier Institute, Hokkaido, Japan), rabbit-Neurogranin (1:500, AB5620, Merck Millipore), mouse-Parvalbumin (1:200, P3088, Sigma-Aldrich), guinea pig-vGluT2 (1:500, VGluT2-GP-Af810, Frontier Institute), guinea pig-PSD-95 (1:200, PSD95-GP-Af660, Frontier Institute), rabbit-GluD2 (1:200, GluD2C-Rb-Af1200, Frontier Institute), guinea pig-Car8 (1:200, Car8-GP-Af500, Frontier Institute), Rat-GFP (1:1000, #06083-05, Nacalai Tesque), Rabbit-Mef2c (1:500, D80C1, Cell Signaling Technology), guinea pig-CaV2.1 (1:200, VDCCa1A-GP-Af810, Frontier Institute), rabbit-SHH (1:200, sc-9024, Santa Cruz) and goat-GLI1 (1:500, sc-6153, Santa Cruz). The tissue sections were subsequently labeled with secondary antibodies conjugated with Alexa Fluor 488, Alexa Fluor 568 or Alexa Fluor 647 (1:1000, abcam, Cambrige, UK). Cell nuclei were labeled with DAPI (1:3000, Thermo Fisher Scientific, Waltham, MA, USA) and for immunohistochemistry of AUTS2, antigen retrieval was performed using Target Retrieval Solution (Dako, Carpinteria, CA, USA) in a boiling jar pot for 20 min according to manufacturer's procedure. For immunostaining of PSD-95 and GluD2, the tissue sections were pre-treated with 0.2 mg/ml pepsin in 0.2N HCl for 20 min before primary antibody reaction as previously described with modifications (Fukaya and Watanabe, 2000; Yamasaki et al., 2011). Fluorescent images were acquired with a laser scanning confocal microscope (FV1000, Olympus, Tokyo, Japan) or Zeiss LSM 780 confocal microscope system and ZEN software (Carl Zeiss, Oberkochen, Germany). For Nissl staining, sections were stained with 0.1 % cresyl violet in 1 % acetic acid, dehydrated with ethanol series, mounted in Entellan, and observed with a Keyence All-in-One microscope (BZ-X700, Osaka, Japan). The cerebellar area, the number of PCs, dendritic height and diameter, the height and puncta number of vGluT2 and fluorescence intensities for GluD2-immunosignals were

measured with Fiji software. For measurements of the height and puncta number of vGluT2, puncta with sizes greater than 0.5 μm^2 were defined as vGluT2-positive CF presynapses whereas puncta smaller than 0.5 μm^2 or located outside the dendritic shafts were considered as background noise (Miyazaki et al., 2004). The density of GluD2 puncta was automatically measured and calculated using "Trainable Weka segmentation", "Auto Threshold "and "Analyze Particles" modules in Fiji software with modification.

Immunoblotting

For the detection of endogenous AUTS2 in the cerebellum, whole cerebella were solubilized with SDS sample buffer, and boiled at 95 °C for 5 min. Whole cerebella lysates (1 mg) were fractionated by SDS-PAGE, and transferred onto a nitrocellulose membrane (Bio-Rad, Hercules, California, USA), immunoblotted with primary antibodies including rabbit-AUTS2 (1:500, HPA000390, Sigma-Aldrich, St. Louis, MO, USA), rabbit-GAPDH (1:1000, 2118S, Cell Signaling Technology), and then visualized using HRP-conjugated secondary antibody (GE Healthcare, Chicago, IL, USA) followed by ECL prime (GE Healthcare, Chicago, IL, USA).

For the evaluation of knockdown efficacy, HEK293T cells were simultaneously transfected with or without pCL20c-trL7, *Auts2* miRNA, FL-AUTS2, S-AUTS2-Var1 and Var2 using Lipofectamine LTX Reagents (15338100, Invitrogen) according to manufacturer's instructions. At 36-48 hrs after transfection, cells were harvested, solubilized with SDS sample buffer and boiled at 95 °C for 5 min. Samples were fractionated by SDS-PAGE with NextPage III gradient gels (GLX-3YGM, Gellex, Tokyo, Japan), transferred to nitrocellulose membranes, immunoblotted with primary antibodies including rabbit-AUTS2 (1:500) and mouse-β-Actin (1:1000, 6D1, MBL, Nagoya, Japan) and visualized with HRP-conjugated secondary antibody. Images were acquired by a cooled CCD camera (LAS-4000 mini; Fujifilm, Kanagawa, Japan).

Golgi staining

Whole brains were subjected to Golgi impregnation solution (FD Rapid GolgiStain kit, FD NeuroTechnologies, Columbia MD, USA). Parasagittal sections at 80-100 μm thickness were prepared with cryostat (CM3050S, Leica, Germany) and mounted on gelatin-coated slides. Golgi-Cox staining was performed according to manufacturer's instructions. The sections were dehydrated with an ethanol series and embedded in Entellan (Merck, Darmstadt, Germany). After z-stack images of dendritic spines were captured using 3-zoom mode of Keyence microscope with a 100x oil-immersion objective, the length of dendrite and number of spines were manually quantified

using Fiji software.

Quantitative RT-PCR

Total RNA from whole cerebella at P7 was purified with the Qiagen RNeasy Plus Universal mini kit (Qiagen, Hilden, Germany). One μg of purified RNA was reverse transcribed to cDNA using the ReverTra Ace qPCR RT kit (Toyobo, Osaka, Japan). Real-time qPCR was performed with PowerUp SYBR Green Master Mix (Thermo Fisher Scientific, Waltham, MA, USA) with the Light Cycler® 96 system (Roche, Basel, Switzerland). The relative expression was calculated via the 2Δ method and normalized to β-actin as the internal control. Primer sequences are as follows: *Rora*, fwd 5′-GTGGAGACAAATCGTCAGGAAT-3′ and rev 5′-TGGTCCGATCAATCAAACAGTTC-3′; *Cacna1a*, fwd 5′- CACCGAGTTTGGGAATAACTTCA-3′ and rev 5′- ATTGTGCTCCGTGATTTGGAA-3′; *Actb*, fwd 5′-GGCTGTATTCCCCTCCATCG-3′ and rev 5′- CCAGTTGGTAACAATGCCATGT-3′.

***In utero* electroporation (IUE)**

IUE experiments were performed as previously described (Takeo et al., 2015). In brief, pregnant C57BL/6 mice at E11.5 or E12.5 obtained from CLEA Japan (Tokyo, Japan) and Japan SLC (Tokyo, Japan) were deeply anesthetized with sodium pentobarbital (50-60 μg/g of body weight, intraperitoneal injection). Plasmid DNAs were dissolved in HEPES-buffered saline at a final concentration of 1-2 μg/μl together with Fast Green (0.3 mg/mL). The plasmid solution (1-3μl) was injected into the fourth ventricle by air pressure under the illumination of a flexible fiber optic light source and electrical pulses (33V, with a duration of 30ms, at intervals of 970 ms per pulse, 5 cycles) were applied with tweezer-type electrodes (CUY650P3; NEPA Gene, Chiba, Japan) and an electroporator (CUY21SC; NEPA Gene, Chiba, Japan).

Electrophysiology

The procedures for electrophysiological recordings have been described previously (Hashimoto and Kano, 2003). Briefly, mice at P21-30 were decapitated under CO_2 anesthesia, and brains were rapidly removed and placed in chilled external solution (0-4°C) containing 125 mM NaCl, 2.5 mM KCl, 2 mM $CaCl_2$, 1 mM $MgSO_4$, 1.25 mM NaH_2PO_4, 26 mM $NaHCO_3$, and 20 mM glucose, bubbled with 95% O_2 and 5% CO_2 (pH 7.4). Parasagittal cerebellar slices (250 μm) were prepared by using a vibratome slicer (VT-1200S, Leica, Germany). Whole-cell recordings were made from visually identified or fluorescent protein-positive using upright and fluorescence microscopes at 32°C (BX50W1, Olympus). We randomly chose the PCs in multiple lobules. Patch pipettes (1.5–2.5 MΩ)

were filled with an intracellular solution composed of (in mM): 60 CsCl, 10 D-gluconate, 20 TEA-Cl, 20 BAPTA, 4 $MgCl_2$, 4 ATP, 0.4 GTP, and 30 HEPES (pH 7.3, adjusted with CsOH) for recording EPSCs; 124 CsCl, 10 HEPES, 10 BAPTA, 1 $CaCl_2$, 4.6 $MgCl_2$, 4 ATP, 0.4 GTP (pH 7.3, adjusted with CsOH) for recording miniature IPSCs (mIPSCs). The pipette access resistance was compensated by 70%. Signals were sampled at 0.1-10 kHz and low-pass filtered at 0.05-2 kHz using an EPC10 patch clamp amplifier (HEKA-Electronik, Lambrecht/Pfalz, Germany). Picrotoxin (100 μM, Nacalai Tesque) and tetrodotoxin (0.5 μM, Nacalai Tesque) were added for recording miniature EPSCs (mEPSCs). NBQX (10 μM, Tocris), R-CPP (5 μM, Tocris) and tetrodotoxin (0.5 μM) were added for recording mIPSCs. Picrotoxin (100 μM) was added to block inhibitory synaptic transmission for recording climbing fiber-induced EPSCs (CF-EPSCs) and parallel fiber-induced EPSCs (PF-EPSCs). Holding potential was -10 mV for CF-EPSCs and -70 mV for PF-EPSCs, mEPSCs and mIPSCs (corrected for liquid junction potential). Stimulation pipettes (5-10 μm tip diameter) were filled with the normal ACSF and used to apply square pulses for focal stimulation (duration of 100 μs, amplitude of 0 V to 100 V). CFs were stimulated in the granule cell layer at positions 20-100 μm away from the PC soma. Single or multiple steps of CF-EPSCs were elicited in a given PC when the intensity of stimulation was increased gradually. The numbers of CFs innervating the recorded PC was estimated based on the number of discrete CF-EPSC steps elicited on that PC (Hashimoto and Kano, 2003). PFs were stimulated in the molecular layer at the position where a maximum response was elicited with the stimulus current of 5 μA. The stimulus intensity was decreased gradually from 5 to 0.5 μA to obtain the input-output curve. Online data acquisition and offline data analysis were performed using PULSE and PULSE FIT software (HEKA-Electronik) or Minianalysis Program ver. 6.0.3 (Synaptosoft Inc, Fort Lee, NJ, USA).

Elevated platform test

Elevated platform tests were carried out as previously described (Alvarez-Saavedra et al., 2014) with modifications. In brief, mice at the ages of 2-4 months were placed in the center of a 10 cm^2 round and 20 cm height elevated platform. The time mice remained on the platform was measured.

Rotarod

Mice at 2-4 months old were placed on an accelerating rod using Rotarod 47600 (Ugo Basile, Italy). After mice were placed on the rod at 4 rpm for 10 sec, the rod was set to accelerate from 4 rpm to 40 rpm over 300 s. Mice were subjected to 3 trials per day for 2 consecutive days with 10 min interval between each trial. The time was measured until they fell from or clung to the rotating drum.

Ultrasonic vocalizations (USVs)

Male mice at 8-15 weeks old were individually housed for a week prior to test time to habituate to the testing environment. Then, an unfamiliar 3 months old C57BL6/N wild type female mouse was placed into the test cage. Recordings started after USVs were detected and continued for 1 min. If USV was not detected for 100 s after male mice met female mice, the number of USVs was regarded as zero. USV recordings were acquired with an UltraSoundGate system (Avisoft bioacoustics, Glienicke, Germany) composed of a CM16/CMPA condenser microphone, Avisoft-UltraSoundGate 116H computer interface, and Avisoft Recorder software with a sampling rate of 400 kHz. The number of and the duration of calls with tone frequencies between 40-170 kHz were automatically measured by MATLAB-based program USVSEG with modification to mouse USVs (Tachibana et al., 2014).

Statistical analysis

Sample size was determined by established methods. Data analyses were performed blinded to the genotype. All statistical analyses were performed by GraphPad Prism 8 (GraphPad Software, La Jolla, CA, USA) and IBM SPSS statistics 21 (IBM SPSS Inc., Chicago, IL, USA). The Shapiro-Wilk test was used for the confirmation of the normal distribution and if significant, a nonparametric Mann Whitney U test was applied for comparison. In case of comparison between two groups, the data within normal distribution and equal variance were analyzed using a two-tailed unpaired t-test. If equal variance of the data was significantly different, we used a two-tailed unpaired t-test with Welch's correction. In case of comparison of more than two groups, two-way ANOVA followed by Bonferroni's multiple comparisons test.

Supplemental References

Alvarez-Saavedra, M., De Repentigny, Y., Lagali, P.S., Raghu Ram, E.V., Yan, K., Hashem, E., Ivanochko, D., Huh, M.S., Yang, D., Mears, A.J., *et al.* (2014). Snf2h-mediated chromatin organization and histone H1 dynamics govern cerebellar morphogenesis and neural maturation. Nat Commun *5*, 4181.

Fukaya, M., and Watanabe, M. (2000). Improved immunohistochemical detection of postsynaptically located PSD-95/SAP90 protein family by protease section pretreatment: a study in the adult mouse brain. J Comp Neurol *426*, 572-586.

Sawada, Y., Kajiwara, G., Iizuka, A., Takayama, K., Shuvaev, A.N., Koyama, C., and Hirai, H. (2010).

High transgene expression by lentiviral vectors causes maldevelopment of Purkinje cells in vivo. Cerebellum *9*, 291-302.

Tachibana, R.O., Oosugi, N., and Okanoya, K. (2014). Semi-automatic classification of birdsong elements using a linear support vector machine. PLoS One *9*, e92584.